Volatile and light lithophile elements in high-anorthite plagioclase-hosted melt inclusions from Iceland

David A. Neave [a,b,*], Margaret E. Hartley [c], John Maclennan [b], Marie Edmonds [b], Thorvaldur Thordarson [d]

[a] *Leibniz Universität Hannover, Institut für Mineralogie, Callinstraße 3, 30173 Hannover, Germany*
[b] *Department of Earth Sciences, University of Cambridge, Downing Street, Cambridge CB2 3EQ, United Kingdom*
[c] *School of Earth and Environmental Sciences, University of Manchester, Oxford Road, Manchester M13 9PL, United Kingdom*
[d] *Faculty of Earth Sciences, University of Iceland, Askja, Sturlugata 7, 101 Reykjavík, Iceland*

Abstract

Melt inclusions formed during the early stages of magmatic evolution trap primitive melt compositions and enable the volatile contents of primary melts and the mantle to be estimated. However, the syn- and post-entrapment behaviour of volatiles in primitive high-anorthite plagioclase-hosted melt inclusions from oceanic basalts remains poorly constrained. To address this deficit, we present volatile and light lithophile element analyses from a well-characterised suite of nine matrix glasses and 102 melt inclusions from the 10 ka Grímsvötn tephra series (i.e., Saksunarvatn ash) of Iceland's Eastern Volcanic Zone (EVZ). High matrix glass H_2O and S contents indicate that eruption-related exsolution was arrested by quenching in a phreatomagmatic setting; Li, B, F and Cl did not exsolve during eruption. The almost uniformly low CO_2 content of plagioclase-hosted melt inclusions cannot be explained by either shallow entrapment or the sequestration of CO_2 into shrinkage bubbles, suggesting that inclusion CO_2 contents were controlled by decrepitation instead. High H_2O/Ce values in primitive plagioclase-hosted inclusions (182–823) generally exceed values expected for EVZ primary melts (∼180), and can be accounted for by diffusive H_2O gain following the entrainment of primitive macrocrysts into evolved and H_2O-rich melts a few days before eruption. A strong positive correlation between H_2O and Li in plagioclase-hosted inclusions suggests that diffusive Li gain may also have occurred. Extreme F enrichments in primitive plagioclase-hosted inclusions (F/Nd = 51–216 versus ∼15 in matrix glasses) possibly reflect the entrapment of inclusions from high-Al/(Al + Si) melt pools formed by dissolution-crystallisation processes (as indicated by HFSE depletions in some inclusions), and into which F was concentrated by uphill diffusion since F is highly soluble in Al-rich melts. The high S/Dy of primitive inclusions (∼300) indicates that primary melts were S-rich in comparison with most oceanic basalts. Cl and B are unfractionated from similarly compatible trace elements, and preserve records of primary melt heterogeneity. Although primitive plagioclase-hosted melt inclusions from the 10 ka Grímsvötn tephra series record few primary signals in their volatile contents, they nevertheless record information about crustal magma processing that is not captured in olivine-hosted melt inclusions suites.
© 2017 The Author(s). Published by Elsevier Ltd. This is an open access article under the CC BY license (http://creativecommons.org/licenses/by/4.0/).

Keywords: Plagioclase-hosted melt inclusions; Volatiles; Primitive basalt; Diffusion; Magma mixing; Iceland

* Corresponding author at: Leibniz Universität Hannover, Institut für Mineralogie, Callinstraße 3, 30173 Hannover, Germany.
 E-mail address: d.neave@mineralogie.uni-hannover.de (D.A. Neave).

1. INTRODUCTION

Mantle melts are modified by a range of mixing, fractionation and assimilation processes as they rise towards

the Earth's surface (O'Hara, 1968; Duncan and Green, 1987; Langmuir et al., 1992; Rubin et al., 2009; Shorttle, 2015). Petrological records of mantle melting and magmatic evolution are thus progressively degraded as magmas ascend and differentiate. This degradation is particularly severe in the case of the volatile species (H_2O, CO_2, F, S and Cl) that exsolve and become decoupled from non-volatile species when melts reach vapour saturation (Stolper and Holloway, 1988; Dixon and Stolper, 1995). Melt inclusions – pools of silicate liquid partially insulated from changes in the external magmatic environment by their host crystals – thus represent appealing targets for investigating the behaviour of magmatic volatiles (Anderson and Brown, 1993; Sobolev and Chaussidon, 1996; Métrich and Wallace, 2008). However, before interpreting melt inclusion compositions in terms of primary magmatic processes, it is imperative to assess the degree to which they have been modified by secondary processes. That is, geochemical variability in melt inclusion suites must be interpreted in terms of syn- and post-entrapment processes as well as pre-entrapment processes.

Possible mechanisms for modifying inclusion compositions during entrapment include the accumulation of slowly diffusing elements such as Al, Cl and S against rapidly growing crystals faces resulting in the entrapment of Al-, Cl- and S-enriched boundary layers (Faure and Schiano, 2005; Baker, 2008). However, unambiguous examples of such diffusive pile-up in natural samples are rare, and the importance of this process in melt inclusion formation remains uncertain (Kent, 2008). Geochemically anomalous melt inclusions in plagioclase macrocrysts have nonetheless been accounted for by the incomplete re-equilibration of melt channels and boundary layers generated by dissolution-crystallisation processes during inclusion formation (Nakamura and Shimakita, 1998; Michael et al., 2002).

Prior to final cooling, inclusions commonly experience post-entrapment crystallisation (PEC) (Roedder, 1979; Kress and Ghiorso, 2004). While PEC acts to simply concentrate most volatiles because of their largely incompatible characters – though Newcombe et al. (2014) describe how PEC can induce intra-inclusion heterogeneity – its effect on CO_2 is more complex: alongside contrasts in density and thermal expansivity between host crystals and their inclusions, PEC-driven changes in trapped melt compositions lead to the nucleation of shrinkage bubbles (Roedder, 1984; Lowenstern, 1995; Maclennan, 2017). Although shrinkage bubbles probably do not contain appreciable quantities of H_2O (though see Esposito et al., 2016), they can sometimes sequester significant amounts of CO_2, and must therefore be considered when estimating the total CO_2 content of melt inclusions (Steele-Macinnis et al., 2011; Bucholz et al., 2013; Hartley et al., 2014; Sides et al., 2014; Moore et al., 2015; Wallace et al., 2015). Melt inclusion CO_2 contents can also be affected by decrepitation when pressure differences between inclusions and the external environment exceed the strength of host crystals, causing them to rupture and leak (Tait, 1992; Schiano, 2003; Maclennan, 2017).

Given sufficient time, melt inclusions can also respond to changes in their magmatic environment by diffusive re-equilibration (Qin et al., 1992). Although few melt inclusions show evidence for the re-equilibration of slowly diffusing incompatible trace elements (ITEs; Cottrell et al., 2002), many olivine-hosted inclusions show evidence for the exchange of rapidly diffusing H^+ (Massare et al., 2002; Koleszar et al., 2009; Chen et al., 2013; Lloyd et al., 2013). Indeed, the re-equilibration of H^+ through olivine hosts typically occurs within hours to days in basaltic systems (Portnyagin et al., 2008; Gaetani et al., 2012), providing a useful chronometer for pre-eruptive magma mixing processes (Bucholz et al., 2013; Le Voyer et al., 2014; Hartley et al., 2015). Although OH^- loss from plagioclase macrocrysts has been reported in magmas undergoing progressive H_2O degassing (Hamada et al., 2011), the susceptibility of plagioclase-hosted melt inclusions to H species re-equilibration remains to be clarified.

To date, most studies on melt inclusions from oceanic basalts have focused on olivine for three main reasons: firstly, early-forming olivine macrocrysts are abundant in mafic rocks (e.g., Roeder and Emslie, 1970; Kent, 2008); secondly, olivine-melt equilibria are comparatively simple, making PEC corrections tractable (e.g., Ford et al., 1983; Toplis, 2005; Danyushevsky and Plechov, 2011); and thirdly, olivine is thought to be a more robust than highly cleaved plagioclase and clinopyroxene. However, many erupted magmas contain significantly more plagioclase than olivine (Flower, 1980; Sinton et al., 1993; Nielsen et al., 1995; Lange et al., 2013; Neave et al., 2014b), and plagioclase-hosted melt inclusions may offer the only means of sampling primitive melt compositions; olivine-hosted inclusions may be too small to analyse or simply absent. While high-anorthite plagioclase-hosted melt inclusions may preserve comparable records to high-forsterite olivine-hosted inclusions (Sours-Page et al., 2002; Font et al., 2007), the processes that modify plagioclase-hosted melt inclusion compositions are, with the exceptions of PEC and dissolution-crystallisation (Nielsen et al., 1995, 1998; Nakamura and Shimakita, 1998; Michael et al., 2002; Adams et al., 2011), poorly understood (Kent, 2008). Analyses of multiple volatiles in plagioclase-hosted inclusions from MORB and OIB settings are particularly rare (cf., Helo et al., 2011), and evaluations of the processes controlling their abundances rarer still.

Here we aim to identify the primary and secondary controls on the volatile and light lithophile element contents of primitive plagioclase-hosted melt inclusions from an oceanic setting. We report analyses of Li, B, F, S and Cl in matrix glasses and mainly plagioclase-hosted melt inclusions from the Icelandic 10 ka Grímsvötn tephra series whose H_2O, CO_2, major element and trace element systematics have been investigated by Neave et al. (2015). Although we find that few primary magmatic signals are preserved in the volatile content of primitive-plagioclase-hosted melt inclusions, compositional variability related to syn- and post-entrapment modification processes nevertheless offers insights into magma evolution that are obscured from olivine-hosted records.

2. THE 10 KA GRÍMSVÖTN TEPHRA SERIES (I.E., SAKSUNARVATN ASH)

2.1. Geological setting

The tephra horizon commonly referred to as the Saksunarvatn ash occurs across the North Atlantic from Greenland to Germany (Waagstein, 1968; Mangerud et al., 1986; Grönvold et al., 1995; Bramham-Law et al., 2013). The tephra, named after its type locality in the Faroe Islands, forms an important tephrochronological marker in sediment and ice cores across the region (e.g., Thornalley et al., 2011). Tephra glasses are compositionally allied with the Grímsvötn volcanic system in southern Iceland (Fig. 1; Grönvold et al., 1995; Jennings et al., 2014), and with magmatic tephra glasses from the voluminous and environmentally impacting AD 1783–1784 Laki eruption in particular (Neave et al., 2015). The Saksunarvatn ash horizon is composed of tephra from at least six eruptions that took place between 10.5 ka and 9.9 ka, and ranged in volume from >1 to 30 km^3 (Jóhannsdóttir et al., 2005; Jennings et al., 2014; Thordarson, 2014). We refer to these collected tephra layers as the 10 ka Grímsvötn tephra series in order to distinguish them from the Saksunarvatn ash proper on the Faroe Islands.

2.2. Petrological context

Proximal samples of the 10 ka Grímsvötn tephra series contain abundant high-anorthite plagioclase macrocrysts, which in turn contain abundant glassy melt inclusions, making them well suited for investigating plagioclase-hosted inclusions (Fig. 2): complex re-homogenisation procedures can be avoided. Rare inclusion-bearing olivines are also present.
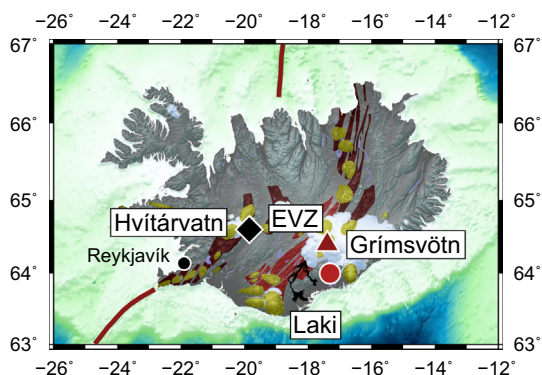

Fig. 1. Map showing the location of Hvítárvatn where samples of the 10 ka Grímsvötn tephra series were collected (black diamond). The tephra series is compositionally associated with the Grímsvötn volcanic system (red triangle) and the Laki eruption in particular (lava field outline shown in black). Grímsvötn is located in the volcanically productive Eastern Volcanic Zone (EVZ; shaded in bright red), where the Mid-Atlantic Ridge makes is closest approach to the centre of the Iceland plume (red circle; Shorttle et al., 2010). Neovolcanic zones outside the EVZ are shaded in dark red and central volcanoes are shaded in yellow. (For interpretation of the references to colour in this figure legend, the reader is referred to the web version of this article.)

There are two discrete macrocryst assemblages in the tephra (Neave et al., 2015): an evolved assemblage of small macrocrysts and macrocryst rims (An_{60}–An_{68}, $Mg\#_{cpx} = 71$–78, Fo_{70}–Fo_{76}) that are close to being in equilibrium with the matrix glass, and a primitive assemblage of high-anorthite plagioclase (An_{78}–An_{92}), high-Mg# clinopyroxene ($Mg\#_{cpx} = 82$–87) and high-forsterite olivine (Fo_{80}–Fo_{87}) macrocryst cores that are not. This disequilibrium is also reflected in the assemblages' respective ITE contents: evolved glasses are more enriched (mean La/Yb = 3.6) than primitive melt inclusions (mean La/Yb = 2.1). This juxtaposition of disequilibrium assemblages reflects the entrainment of primitive and, on average, ITE-poor mushes into evolved and ITE-enriched melts shortly before eruption (e.g., Halldórsson et al., 2008; Neave et al., 2014b). Nonetheless, significant variability in primitive melt inclusion ITE ratios indicates that the primitive assemblage was assembled from compositionally diverse primary melts (e.g., Maclennan, 2008; Neave et al., 2013). Barometric calculations place magma assembly within the mid crust (2.6–3.1 kbar; 7.4–8.9 km), though some further evolution may have occurred during ascent (Neave et al., 2015; Neave and Putirka, 2017).

2.3. Sample selection and preparation

We report analyses from the samples described previously by Neave et al. (2015): 150–800 μm glass and macrocryst fragments selected from the Saks-eq II HVT layer of the 10 ka Grímsvötn tephra series in the GLAD-HVT03-1A-7H core collected from Lake Hvítárvatn in 2003 (Fig. 1). Saks-eq II HVT is compositionally representative of the tephra series (Neave et al., 2015), and dates to approximately 10.35 ka (Jóhannsdóttir, 2007). The tephra consists primarily of variably vesicular holohyaline clasts alongside abundant plagioclase fragments. Fragments of olivine and clinopyroxene also occur, but are comparatively rare.

Glass and macrocryst fragments were cleaned in distilled water before being mounted in Buehler EpoThin^{TM} resin and polished to expose melt inclusions (Neave et al., 2015). The samples were subsequently re-polished after a first round of analyses in order to expose new melt inclusions and maximise the number of measurements possible with the limited volume of sample material available. Before carrying out any analyses, melt inclusions were filtered optically for signs of extensive PEC (the presence of daughter crystals), decrepitation (cracks or chains of fluid inclusions extending from inclusion walls) and connection to the external environment. Samples were not coated with carbon prior to SIMS analyses to minimise contamination.

3. ANALYTICAL METHODS

3.1. Secondary ion mass spectrometry (SIMS)

SIMS analyses were performed at the NERC Ion Microprobe Facility at the University of Edinburgh, UK, using a Cameca ims-4f instrument. The CO_2 analyses reported by
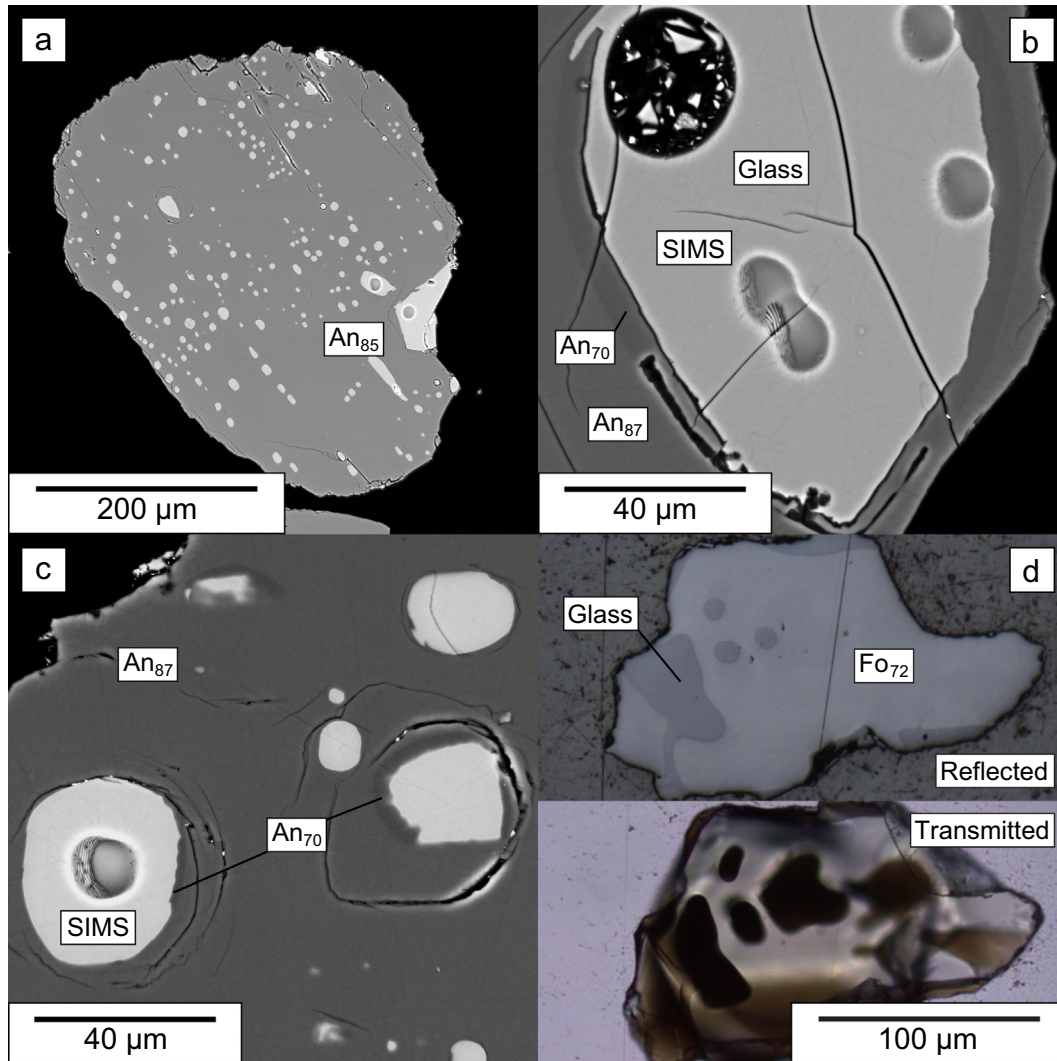
Fig. 2. (a–c) Backscattered electron (BSE) images of high-anorthite macrocrysts and their abundant melt inclusions. Dark low-anorthite (An_{70}) haloes around melt inclusions are particularly visible in (b) and (c). Note the dendritic nature of the low-anorthite growths within melt inclusions. SIMS craters are marked. (d) Evolved olivine containing small melt inclusions.

Neave et al. (2015) were the first made on all samples. Li, B, F and Cl were then measured alongside the H_2O and trace element analyses that are also reported by Neave et al. (2015). Li was only measured in the second of two analytical sessions. Measurements were made using a primary O^- ion beam with an accelerating voltage of 15 kV, a beam current of 6 nA, a 25 µm image field and a secondary accelerating voltage of 4500 V minus a 75 V offset. Analyses were performed with a spot size of ∼15 µm centred in the pit formed during the preceding analyses of CO_2. In addition to elements listed by Neave et al. (2015), the following isotopes were measured for 8 cycles (counting times in seconds in parentheses): $^{7}Li(5)$, $^{11}B(5)$, $^{19}F(10)$ and $^{35}Cl(10)$. Peak positions were verified before each analysis, and the masses 0.7 and 130.5 were measured to determine backgrounds in each cycle. Backgrounds were always sufficiently close to zero to be ignored.

Li and B concentrations were calculated following the principles discussed by Hinton (1990) using the in-house JCION-6 software and NIST-610 as the primary calibration standard (Jochum et al., 2011). Matrix corrections for Li and B were then applied using the synthetic basalt standard GSD-1G (Jochum et al., 2006). Analyses of the standards ML3B-G and KL2-G indicate that accuracy was better than 10% for Li and better than 20% for B (Jochum et al., 2006). Owing to halogen analyses being strongly affected by matrix effects, calibrations for F and Cl were derived from measurements of the standards GSD-1G, BCR-2G, ML3B-G and KL2-G performed across several sessions (Jochum et al., 2006; Guggino, 2012; Marks et al., 2016). Accuracy was estimated to be better than 10% for F and Cl based on the standard errors of regressions used for calibration. The following estimates of analytical precision (1σ) were determined from repeat

analyses of standard and unknown glasses: Li, ±2.0%; B, ±1.8%; F, ±3.2%; and Cl, ±14%.

3.2. Electron probe microanalysis (EPMA)

EPMA was performed at the Department of Earth Sciences at the University of Cambridge, UK, using a Cameca SX100 instrument. F and S were measured concurrently with the major element analyses reported by Neave et al. (2015). Cl was below the detection limit of EPMA. Analyses were made with either 5 μm or 10 μm spot sizes depending on melt inclusion dimensions. In 5 μm spots, S was measured using the same conditions as the major elements: an operating potential of 15 kV with a beam current of 10 nA. F was not measured in 5 μm spots. In 10 μm spots, both F and S were measured using a second condition beam current of 100 nA in order to improve count rates. Fluorite and pyrite were used as calibration standards for F and S respectively. Accuracy was estimated to be better than 15% and 5% for F and S receptively based on measurements of the basaltic glass standard NMNH 113498–1 (A-99) over several sessions (Jarosewich et al., 1980;

Thordarson et al., 1996). The following estimates of analytical precision (1σ) were determined using repeat analyses of unknown glasses: F, ±5.2%; and S, ±3.6%.

A positive correlation between F determined by SIMS and EPMA ($F_{SIMS} \approx 1.1 \times F_{EPMA}$; $r^2 = 0.67$; $p \ll 0.01$) indicates that the two methods are consistent to within 10% (Supplementary Fig. 1), and that the higher precision SIMS data can be used in preference to the EPMA data. T- and F-tests performed on S data collected using 5 μm and 10 μm spot sizes reveal no significant differences in composition distributions between the two analytical conditions, which were thus merged.

4. RESULTS

4.1. Summary of major and trace element compositions

The major and trace element compositions of matrix glasses and melt inclusions from the 10 ka Grímsvötn tephra series were described in detail by Neave et al. (2015). Key features of their dataset, are summarised in Fig. 3, and a full suite of major element variation diagrams
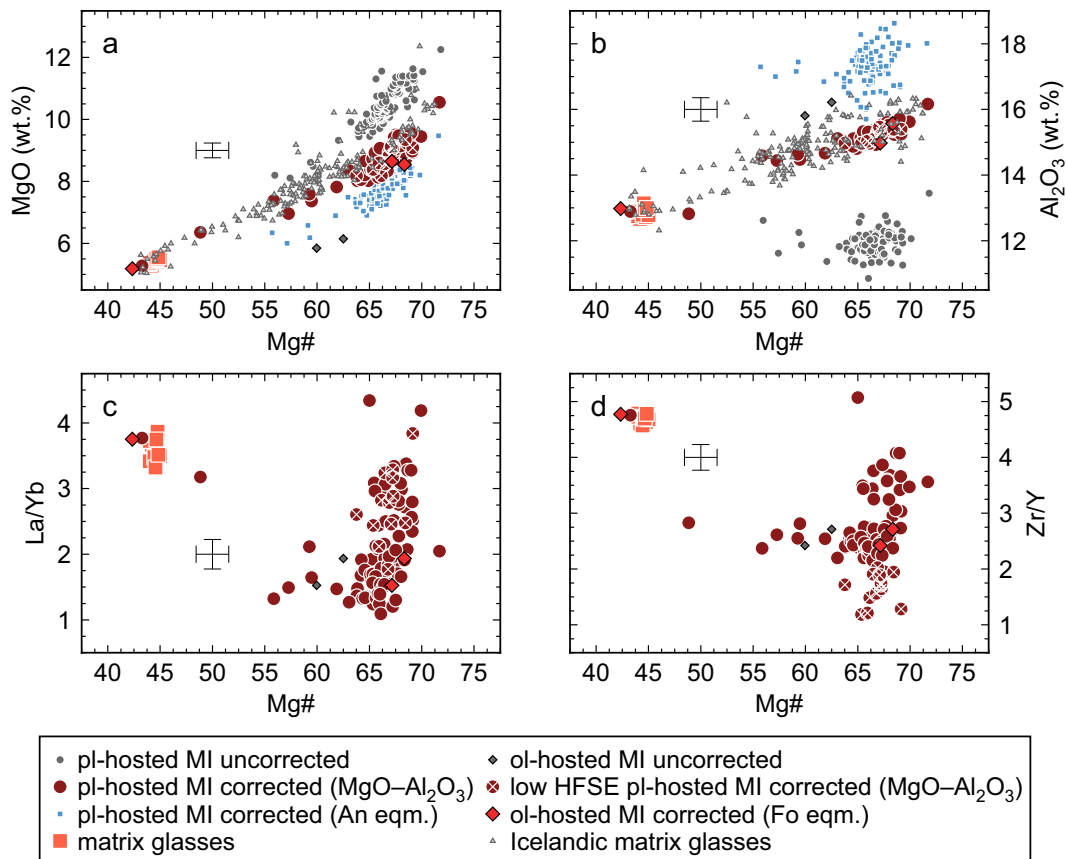

Fig. 3. Plots summarising the major and trace element systematics of matrix glasses and melt inclusions from the 10 ka Grímsvötn tephra series. Raw melt inclusion data from Neave et al. (2015) are plotted using small grey symbols (circles and diamonds for plagioclase- and olivine-hosted melt inclusions respectively). Plagioclase-hosted melt inclusions corrected for post-entrapment crystallisation (PEC) by adding equilibrium plagioclase until inclusion MgO–Al$_2$O$_3$ systematics matched those of Icelandic glasses are plotted using red circles (MgO–Al$_2$O$_3$). Plagioclase-hosted melt inclusions corrected to achieve equilibrium with their host grains are plotted using blue squares (An eqm.). PEC-corrected olivine hosted melt inclusions are plotted using red diamonds (Fo eqm.). Further details about PEC corrections are provided in the main text. Icelandic matrix glass compositions compiled by Shorttle and Maclennan (2011) are shown for reference. 2σ error bars are shown on all plots. (For interpretation of the references to colour in this figure legend, the reader is referred to the web version of this article.)

is provided in Supplementary Fig. 2. Melt inclusion compositions described in this section have been not corrected for PEC; PEC is discussed explicitly in the following section on the modification of melt inclusion compositions.

Matrix glass compositions ($n = 9$) are homogeneous – variations in Mg# and La/Yb do not exceed estimates of analytical precision – and are very similar to previously published compositions from the tephra series (e.g., Mangerud et al., 1986; Grönvold et al., 1995; Bramham-Law et al., 2013). Note that an $Fe^{2+}/\Sigma Fe$ of 0.85 was assumed when calculating Mg# (Shorttle et al., 2015). Two inclusions hosted in evolved macrocrysts have very similar compositions to the matrix glasses.
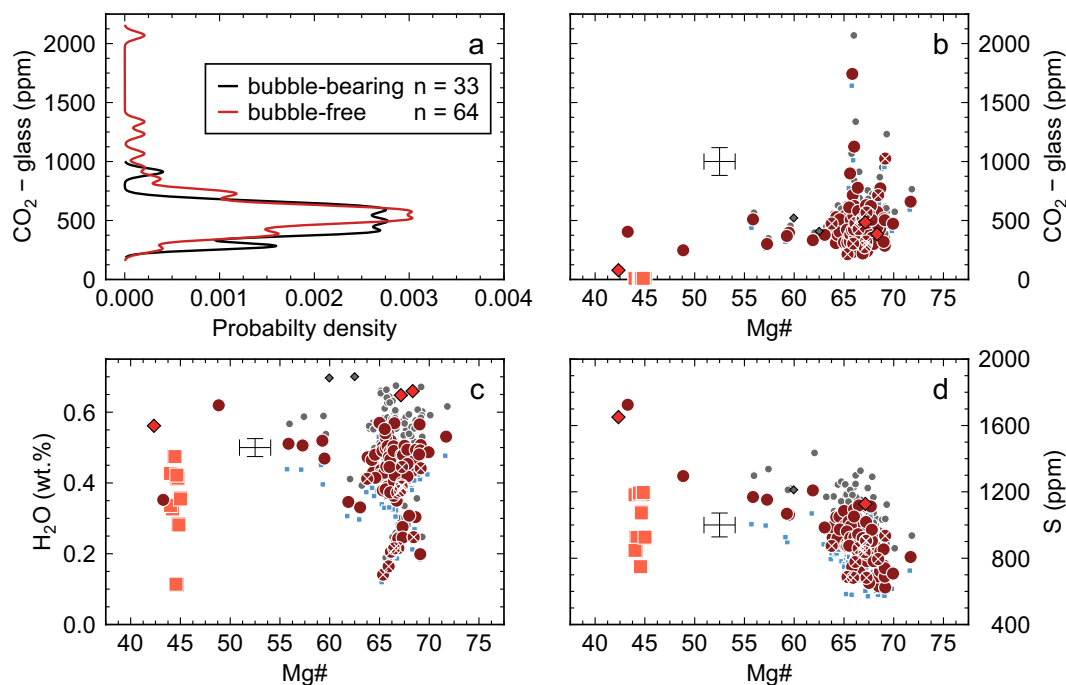
High-anorthite plagioclase-hosted melt inclusions (Fig. 2; An_{78}–An_{92}; $n = 96$) are much more compositionally variable than the matrix glasses. Melt inclusion MgO contents span the range 8.1–12.3 wt.% (Mg# = 56–72), though most inclusions contain 10–11 wt.% MgO (Fig. 3a) and and all bar two high-Mg# inclusions have Al_2O_3 contents in the 10.9–13.4 wt.% range (Fig. 3b). All major elements apart from SiO_2 exhibit significant variability at $p < 0.05$, i.e., signal-to-noise ratios (σ_t/σ_r, where σ_t is the true variation and σ_r is an estimate of analytical precision) exceed the threshold for significant variability calculated using the χ^2 distribution (Maclennan et al., 2003). Melt inclusion trace element systematics are summarised in Fig. 3c and d. In contrast with matrix glasses and evolved melt inclusions, primitive melt inclusions exhibit a large range of La/Yb (1.1–4.3) that is robustly variable at $p < 0.01$. Some inclusions exhibit high field strength element (HFSE) depletions (e.g., Zr/Y < 2 on Fig. 3d) that do not correlate with other geochemical features.

4.2. Volatiles and light lithophile elements

New volatile and light lithophile element analyses are summarised alongside previously published CO_2 and H_2O data from Neave et al. (2015) in Figs. 4 and 5. CO_2 contents are low in evolved melt inclusions (78–405 ppm) and below the detection limit in matrix glasses (~25 ppm). In contrast, the range of CO_2 contents in primitive melt inclusion glasses is large (270–2070 ppm), though CO_2 in most inclusions lies close to the median value of 535 ppm (Fig. 4a and b).

Shrinkage bubbles were investigated by Neave et al. (2015) in order to determine their contributions towards total melt inclusion CO_2 contents (e.g., Steele-Macinnis et al., 2011; Wallace et al., 2015). However, no CO_2 was detected within them, indicating that they contain $\ll 0.04$ g.cm^{-3} CO_2 (Hartley et al., 2014); shrinkage bubbles do not host significant CO_2 in these samples. This restricted partitioning of CO_2 into shrinkage bubbles is further reflected in the similarity of kernel density estimates (KDEs) calculated for the CO_2 contents of bubble-free ($n = 64$) and bubble-bearing ($n = 33$) inclusion populations (Fig. 4a). Furthermore, while some bubble-free inclusions may have lost their bubbles during polishing, bubble-free inclusions are nonetheless abundant beneath polished sample surfaces. We thus assume that melt inclusion glasses contain the inclusions' full CO_2 complements when they quenched. We note that discarding bubble-bearing inclusions has no impact on our subsequent interpretations.

When compared with degassed basaltic tephras from Iceland (e.g., Hartley et al., 2014), matrix glass H_2O contents are high and variable (0.11–0.47 wt.%; Fig. 4c).

Fig. 4. (a) Kernel density estimates (KDEs) of CO_2 in the glass portions of bubble-bearing and bubble-free primitive plagioclase-hosted melt inclusions reported by Neave et al. (2015). Plots summarising the (b) CO_2, (c) H_2O and (d) S contents of matrix glasses and melt inclusions. Symbols are as in Fig. 3. 2σ error bars are shown on all plots.
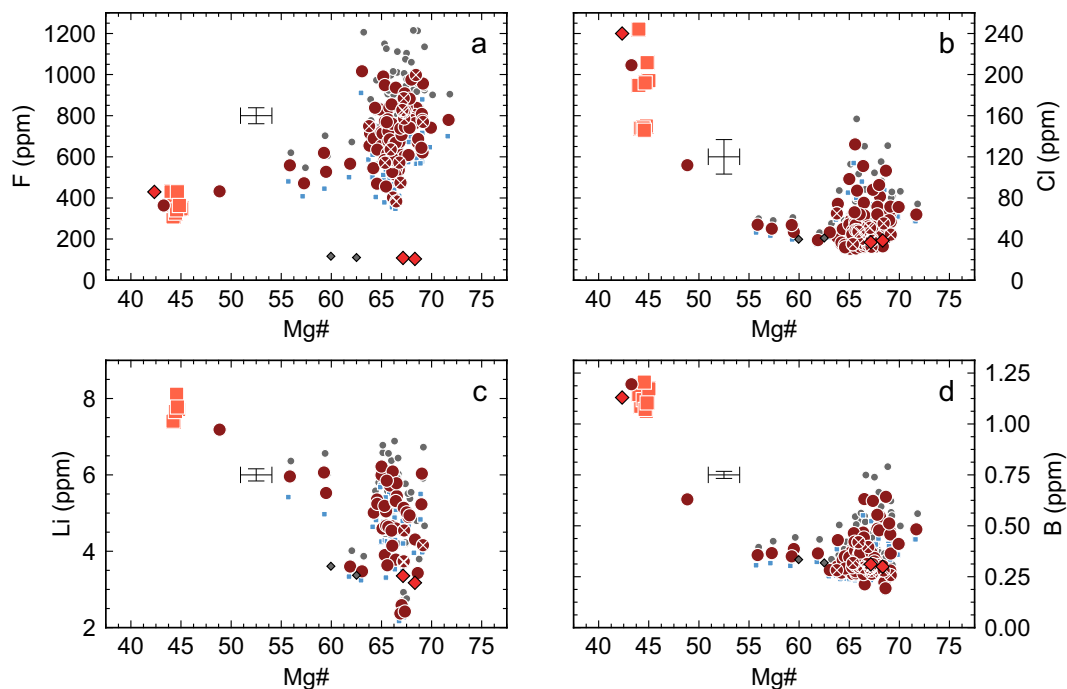
Fig. 5. Plots summarising the (a) F, (b) Cl, (c) Li and (d) B contents of matrix glasses and melt inclusions. Symbols are as in Fig. 3. 2σ error bars are shown on all plots.

Primitive melt inclusion H_2O contents are also high: 0.70 wt.% in the two olivine-hosted inclusions and 0.19–0.68 wt.% in plagioclase-hosted inclusions. Most evolved inclusions are also H_2O-rich (0.56–0.62 wt.%). Matrix glasses have a range of S contents (749–1196 ppm; Fig. 4d), and while primitive melt inclusion S contents are variable (740–1435 ppm), they are generally lower than those of evolved melt inclusions (1295–1650 ppm).

In contrast with their H_2O and S contents, the F, Cl, Li and B contents of matrix glasses are comparatively homogeneous: 308–430 ppm, 146–244 ppm, 7.4–8.1 ppm and 1.06–1.21 ppm respectively (Fig. 5a–d). Evolved melt inclusion compositions also lie within the ranges defined by matrix glasses. However, primitive plagioclase-hosted melt inclusion F, Cl, Li and B contents are highly variable and span the following ranges: F, 460–1215 ppm; Cl, 36.2–156.8 ppm; Li, 2.7–6.9 ppm; and B, 0.23–0.79 ppm. Primitive olivine-hosted melt inclusion Cl, Li and B contents lie within the ranges observed in plagioclase-hosted inclusions: Cl, ~40 ppm; Li, ~3.5 ppm; and B, ~0.33 ppm. Although we cannot define the extent of variability in the small olivine-hosted melt inclusion population, a difference between olivine-hosted and plagioclase-hosted F contents should nonetheless be noted (~113 ppm versus ⩾460 ppm respectively).

5. SYN-ERUPTIVE VOLATILE EXSOLUTION

Matrix glasses from the 10 ka Grímsvötn tephra series contain substantially more H_2O and S (0.11–0.47 wt.% and 749–1196 ppm respectively; Fig. 6a) than degassed magmatic tephra glasses from the geochemically analogous

Laki eruption ($0.08 \pm 0.01(1\sigma)$ wt.% H_2O and $490 \pm 85(1\sigma)$ ppm S; Hartley et al., 2014; Thordarson et al., 1996). Syn-eruptive degassing paths calculated with the D-Compress vapour-melt equilibrium model (Fig. 6a; Burgisser et al., 2015) indicate that most matrix glasses record quenching pressures higher than atmospheric pressure (up to ~10 MPa). Eruption-related degassing was thus arrested prematurely, probably owing to quenching in a phreatomagmatic setting (e.g., Thordarson et al., 1996; Tuffen et al., 2010). Apparent quenching pressures of >1 MPa for most matrix glasses also account for the non-volatile behaviour of F and Cl that typically saturate below ~1 MPa in mafic melts (Carroll and Webster, 1994). Furthermore, Li/Yb values of ~1.7 and strong correlations between B and ITEs in matrix glasses indicate that neither Li nor B were volatile at the time of quenching (Ryan and Langmuir, 1987; Ryan and Langmuir, 1993).

6. POST-ENTRAPMENT MODIFICATION OF MELT INCLUSION COMPOSITIONS

6.1. Post-entrapment crystallisation (PEC) of olivine-hosted melt inclusions

Primitive olivine-hosted melt inclusions experienced substantial PEC during cooling: Mg# = 60–63 inclusions are far from being in equilibrium with their Fo_{86} hosts. Olivine-hosted inclusion compositions were therefore corrected by adding equilibrium olivine back into the melt inclusion compositions until host-inclusion equilibrium was achieved according to the model of Herzberg and O'Hara (2002) combined with the $K_{d\,Fe-Mg}^{ol-liq}$ model of
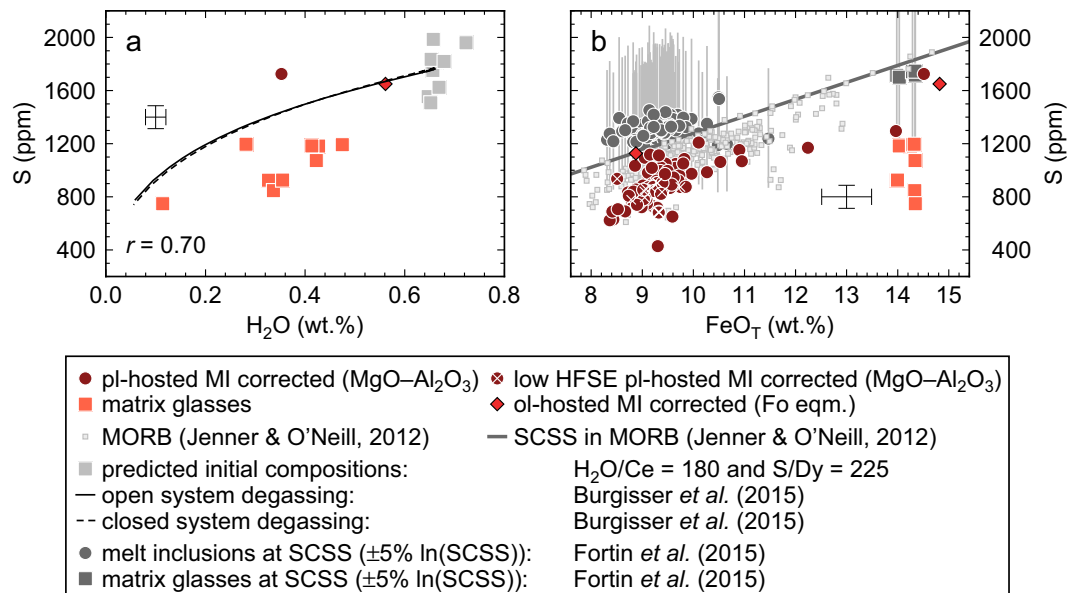
Fig. 6. Plots summarising S systematics in matrix glasses and melt inclusions. (a) H_2O and S contents of matrix glasses and melt inclusions. Matrix glass show a positive correlation between H_2O and S ($r = 0.70; p < 0.05$) that can be largely accounted for by various extents of shallow degassing using D-Compress (Burgisser et al., 2015). D-Compress simulations were performed at 1150 °C in the C-S-O-H-Fe system, with an initial gas fraction of 1%, and fO_2 buffered at QFM. Melt H_2O and CO_2 contents were set to 0.66 wt.% and 700 ppm respectively in order to match melt H_2O/Ce ratios (∼180; Hartley et al., 2015), the S content of evolved melt inclusions (∼1700 ppm), and the depth of final magma equilibration (0–1.5 kbar; Neave et al., 2015). (b) Matrix glass and melt inclusion FeO_T–S systematics shown alongside MORB compositions (Jenner and O'Neill, 2012). Sulphide contents at sulphide saturation (SCSS) are shown for MORB as a function of FeO_T (grey line), as well as for matrix glasses and melt inclusions according to the model of Fortin et al. (2015) (dark grey symbols).

Toplis (2005). Corrections were performed using the reverse crystallisation tool in Petrolog (Danyushevsky and Plechov, 2011); using the PEC correction tool resulted in unacceptably Fe-poor compositions. Corrected melt inclusions have similar Mg#–Al_2O_3 systematics to Icelandic glass compositions (Fig. 3a and b; Shorttle and Maclennan, 2011). Volatile and trace elements were assumed to be perfectly incompatible during PEC correction (e.g., Hauri et al., 2006; Bédard, 2005; Rosenthal et al., 2015). PEC–corrected data are provided in the Supplementary Material.

6.2. PEC of plagioclase-hosted melt inclusions

In their previous investigation, Neave et al. (2015) argued that a combination of high MgO contents and high Mg# values indicate that high-anorthite plagioclase-hosted inclusions from the tephra are genuinely primitive and minimally compromised by PEC. However, further investigation has revealed that plagioclase-hosted inclusions did experience substantial PEC prior to quenching. For example, most inclusions are surrounded by haloes of low-anorthite plagioclase (Fig. 2). By assuming nested, ellipsoidal and symmetrical geometries, typical halo and inclusion dimensions suggest that inclusions experienced ∼15 vol.% PEC (Fig. 2c). Furthermore, at any given Mg#, plagioclase-hosted inclusion MgO and Al_2O_3 contents are respectively 1–2 wt.% higher and 2–4 wt.% lower than the trends defined by Icelandic glasses (Fig. 3a and b; Shorttle and Maclennan, 2011). While the high Mg# of melt inclusions confirms that they are genuinely primitive,

their elevated MgO and depressed Al_2O_3 contents are nonetheless characteristic of PEC (Nielsen, 2011).

Plagioclase-hosted inclusion compositions were thus corrected for PEC by incrementally adding equilibrium plagioclase back into melt inclusion compositions until their MgO–Al_2O_3 systematics were consistent with those of Icelandic glasses (i.e., until Al_2O_3 reached the value predicted from MgO values based on a regression through Icelandic glass data; $r^2 = 0.56; p \ll 0.01$). Equilibrium plagioclase compositions were calculated using the anhydrous plagioclase-melt equilibrium model of Namur et al. (2012); H_2O has only a minor effect on equilibrium anorthite content the concentrations relevant here (<0.7 wt.%; Sisson and Grove, 1993; Panjasawatwong et al., 1995). Trace elements were corrected using the partition coefficients collated by O'Neill and Jenner (2012), and volatiles were assumed to be perfectly incompatible (Johnson, 2005; Dalou et al., 2012).

Correspondence between melt inclusion and Icelandic glass compositions was achieved by adding 10–25 vol.% (median = 16 vol.%) plagioclase to primitive melt inclusion compositions (shown in red on Figs. 3–5), values consistent with observations from BSE images (Fig. 2c). However, melt inclusions are still out of equilibrium with high-anorthite plagioclase after being corrected for ∼16 vol.% of PEC: melt inclusions only reach equilibrium with their hosts after a much more substantial ∼26 vol.% PEC correction (shown in blue on Figs. 3–5).These seemingly discordant estimates of PEC can nonetheless be reconciled via a dissolution-crystallisation mechanism of inclusion

formation that is discussed in detail below. Inclusion compositions corrected to be in equilibrium with Icelandic glasses, which are used in the subsequent discussions, and with their host crystals, which are not, are both provided in the Supplementary Material. However, it is important to note that most elemental ratios used for investigating the behaviour of volatiles in basaltic magmas are unaffected by PEC because both nominator and denominator elements are highly incompatible in plagioclase; our interpretations are robust to uncertainties in PEC corrections.

6.3. Post-entrapment CO_2 loss by decrepitation

To avoid using potentially compromised CO_2–Nb systematics for investigating CO_2 behaviour (some inclusions have HFSE depletions; Neave et al., 2015), we consider CO_2–Ba systematics instead (Fig. 7a; Michael and Graham, 2015). CO_2/Ba values from undegassed Atlantic MORB span the range 66–172, though lie primarily between 100 and 119 (Michael and Graham, 2015), with published estimates of CO_2/Ba in undegassed Icelandic basalts lying to slightly lower values of 79–89 (Hartley et al., 2014; Neave et al., 2014a). Only one melt inclusion from the 10 ka Grímsvötn tephra series has a CO_2/Ba value of 97 that could be primary. Most melt inclusions have low CO_2/Ba values and CO_2 contents that correspond to apparent entrapment pressures of 1–2 kbar (median = 1.4 kbar; Shishkina et al., 2014). However, a pressure of 1–2 kbar is almost certainly too low to represent that of inclusion formation because it is significantly lower than the 3–5 kbar storage pressure estimated using other barometers (Neave et al., 2015; Neave and Putirka, 2017). Furthermore, primitive inclusions are located entirely within macrocryst cores that are not in equilibrium with the matrix glass, and, their
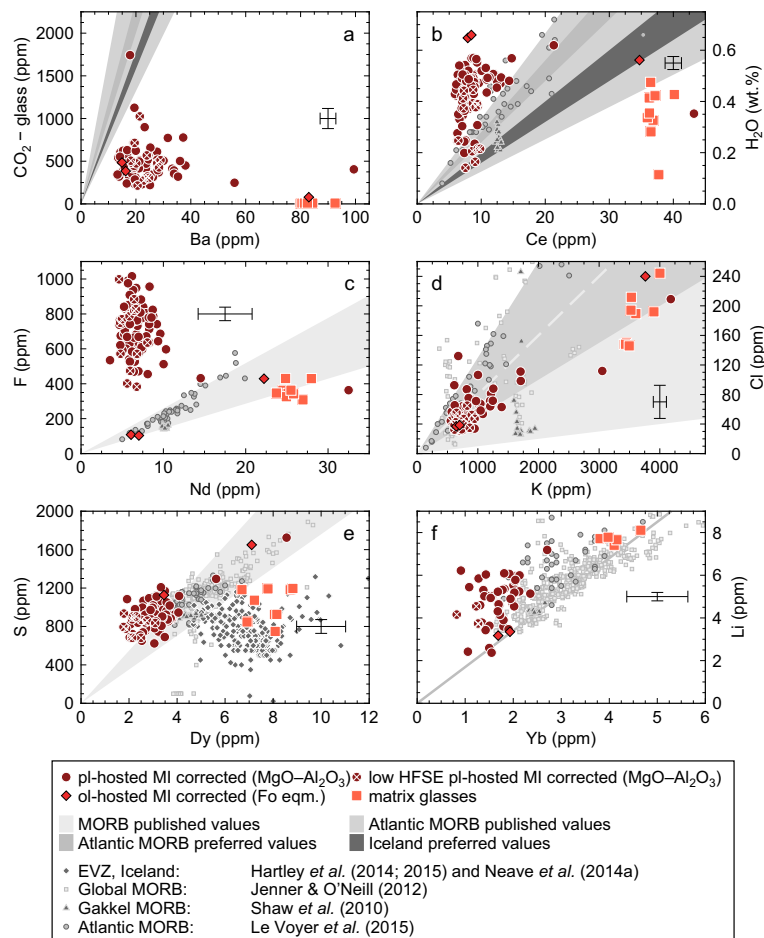

Fig. 7. Plots summarising the combined volatile-trace element systematics in matrix glasses and melt inclusions. (a) CO_2–Ba systematics compared with values from the Mid-Atlantic Ridge (full range in light grey field and preferred values in mid grey field; Michael and Graham, 2015) and Iceland (dark grey field; Hartley et al., 2014; Neave et al., 2014a). (b) H_2O–Ce systematics compared with values from the Mid-Atlantic Ridge (full range in light grey field and preferred values in mid grey field; Michael, 1995) Iceland (dark grey field; Hartley et al., 2015). (c) F–Nd systematics compared with values for oceanic basalts (pale grey field; Workman et al., 2006). (d) Cl–K systematics compared with values for MORB (pale grey field; Michael and Cornell, 1998) and from the Mid-Atlantic Ridge (mid-grey field; Michael and Cornell, 1998). (e) S–Dy systematics compared with values for MORB basalts (pale grey field; Koleszar et al., 2009). (f) Li–Yb systematics compared with a canonical value for oceanic basalts (1.7; grey line; Ryan and Langmuir, 1987).
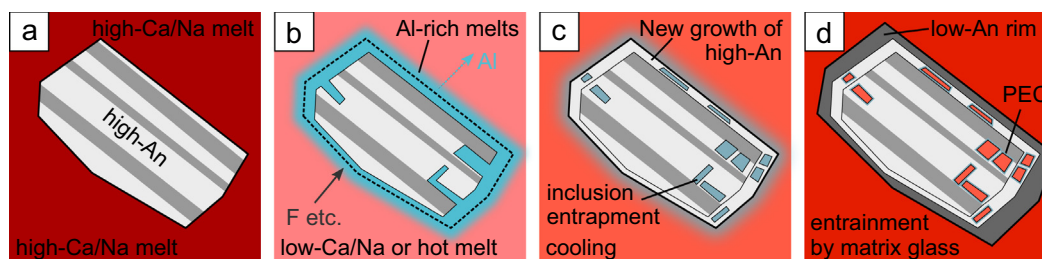
Fig. 8. (a–d) Cartoon illustrating our proposed model of primitive plagioclase-hosted melt inclusion formation. (a) Growth of high-anorthite plagioclase macrocrysts from primitive high-Ca/Na melts. (b) Partial dissolution of high-anorthite plagioclase macrocrysts generates low-HFSE, high-Al/(Al + Si) melts because the sluggish diffusion of Al and HFSEs. F is concentrated into these Al-rich melts by uphill diffusion. (c) Entrapment of melt inclusions by new growth of high-anorthite plagioclase from high-Al/(Al + Si). (d) Entrainment of high-anorthite plagioclase macrocrysts by evolved melts and the growth of low-anorthite rims.

H_2O and Li contents aside (see later), show no evidence of having maintained contact with the external environment during ascent (cf., Blundy and Cashman, 2005).

Although sequestration of CO_2 into shrinkage bubbles can account for low CO_2 contents in some systems (e.g., Hartley et al., 2014; Moore et al., 2015), it cannot in this case because bubble-free and bubble-bearing inclusions have comparable CO_2 contents (Fig. 4a). The distribution of CO_2 contents in plagioclase-hosted melt inclusions does however share many similarities with that in olivine-hosted melt inclusions from Laki the eruption. Namely, most inclusions record entrapment pressures 2–3 kbar lower than pressures estimated using independent barometers (Hartley et al., 2014; Neave and Putirka, 2017). In the case of Laki, this disparity can be accounted for by the decrepitation of melt inclusions reaching overpressures of ~2.5 kbar (Maclennan, 2017). We therefore suggest that post-entrapment rupture may also be responsible for the low entrapment pressures we observe in plagioclase-hosted inclusions: strongly cleaved plagioclase has a lower hardness and tensile strength than weakly cleaved olivine, which could result in decrepitation at overpressures of less than ~2.5 kbar (Tugarinov and Naumov, 1970; van den Kerkhof and Hein, 2001; Bodnar, 2003).

6.4. Post-entrapment H_2O gain by diffusion

H_2O-undegassed melts from the EVZ of Iceland are thought to have primary H_2O/Ce values of 180 ± 20 (Hartley et al., 2015), which are slightly lower than typical Atlantic MORB values of 240–350 (Michael, 1995; Le Voyer et al., 2015), but nonetheless within the range of global values for oceanic basalts (Michael, 1995). While some plagioclase-hosted inclusions have H_2O/Ce values within the primary range (180 ± 20), none have lower values, which is consistent with efficient quenching in a phreatomagmatic setting. Conversely, most plagioclase-hosted inclusions have high H_2O/Ce values of up to 823 that are indicative of open-system H_2O gain by a process that did not affect most other elements; H_2O does not correlate with any element except Li ($r = 0.90; p \ll 0.01$).

Macrocryst zoning patterns and thermobarometric calculations reveal that primitive macrocrysts were entrained by evolved melts shortly before eruption (Neave et al.,

2015). At the conditions of entrainment (~1140 °C and ~3 kbar; Neave et al., 2015; Neave and Putirka, 2017), the average matrix glass would have had an H_2O activity (a_{H_2O}) of ~0.044 assuming that $H_2O/Ce = 180$ (Burnham, 1979). Making the same assumptions, PEC–corrected primitive plagioclase-hosted inclusions would have had a much lower average a_{H_2O} of ~0.002 (or ~0.003 for PEC-uncorrected inclusions). This a_{H_2O} gradient would have provided a drive for inclusions to gain H_2O from the external magmatic environment by diffusion through their host crystals (Hartley et al., 2015).

In order to estimate timescales of olivine-hosted melt inclusion dehydration and overhydration, Hartley et al. (2015) used a modified version of the model presented by Bucholz et al. (2013) for calculating the analytical solution for symmetrical H^+ diffusion through a spherical olivine hosting a spherical melt inclusion at its centre (Qin et al., 1992). Performing equivalent calculations on samples from the 10 ka Grímsvötn tephra series is complicated by the fragmented nature of the ash-borne macrocrysts. Nevertheless, we estimate that the two primitive olivine-hosted melt inclusions would have experienced complete H_2O re-equilibration within 0.5–4.0 days assuming a temperature of 1140 °C, a partition coefficient ($K_{H_2O}^{ol-melt}$) of 0.0007 (Le Voyer et al., 2014), a diffusivity ($D_{H^+[001]}^{ol}$) calculated from Demouchy and Mackwell (2006) and a realistic range of macrocryst radii (100–500 μm). This represents the minimum timescale for primitive macrocryst residence in the evolved melt because re-equilibration has run to completion.

Plagioclase-hosted melt inclusions have variable H_2O contents and H_2O/Ce values, which indicate that re-equilibration was often incomplete. There are two main reasons for this: firstly, high-anorthite plagioclase macrocrysts from Iceland are often much larger than olivine macrocrysts, which increases the diffusion distance (Hansen and Grönvold, 2000; Neave et al., 2014b); and secondly, the diffusion of H^+ though plagioclase is approximately one order of magnitude slower than it is through olivine (Johnson and Rossman, 2013). Following Cassidy et al. (2016), approximate re-equilibration timescales were calculated by assuming a temperature of 1140 °C, a partition coefficient ($K_{H_2O}^{pl-melt}$) of 0.01 (Hamada et al., 2013), a diffusivity ($D_{H^+}^{pl}$)

calculated by extrapolating the model of Johnson and Rossman (2013) to 1140 °C and a range of plausible macrocryst radii (250–4000 μm). Runs were terminated when the modelled H_2O content of each melt inclusion matched its measured H_2O content.

Dominant re-equilibration timescales were determined for each host radius by transforming timescale populations into KDEs (Fig. 8). For a radius of 250 μm, the dominant timescale is ∼0.4 days, which increases to ∼6.1 days for a radius of 4000 μm. Despite the uncertainties in model parameters, and macrocryst sizes in particular, these plagioclase residence time are nonetheless comparable with estimates from olivine-hosted inclusions. They are also consistent with entrainment timescale estimates from the nearby Laki eruption (Hartley et al., 2015; Hartley et al., 2016). In samples with well-constrained macrocryst dimensions, the diffusive exchange of H_2O through plagioclase has considerable potential as a chronometric tool sensitive to pre-eruptive processes on the timescale of days to tens of days.

6.5. Li in melt inclusions: A role for re-equilibration?

Given that Li/Yb values of 1.7–1.9 in the primitive two olivine-hosted melt inclusions are probably primary (Ryan and Langmuir, 1987), it is possible to estimate a maximum timescale for their pre-eruptive residence in evolved liquids by estimating the delay before high Li contents in the external environment would have been transmitted into melt inclusions. Li diffusion though olivine hosts was thus modelled using a partition coefficient ($K_{Li}^{ol-melt}$) of 0.15 (Brenan et al., 1998) and a diffusivity ($D_{Li_{Me/c}}^{ol}$) calculated from Eq. (20) of Dohmen et al. (2010). Using olivine radii of 100–500 μm, we calculate a maximum residence timescale of 2.4–128 days.

The strong correlation between H_2O and Li in primitive plagioclase-hosted melt inclusions ($r = 0.90; p \ll 0.01$) sug-gests that Li may have also diffused into these melt inclusions. However, modifying the model used for H_2O re-equilibration calculations results in implausibly short timescales (minutes to hours) because of Li's relative compatibility in and fast diffusion through plagioclase (Giletti and Shanahan, 1997; Johnson and Rossman, 2013; Dohmen and Blundy, 2014). However, given the absence of H_2O- and Li-rich but otherwise ITE-depleted primitive melts from the Icelandic geological record, the strong correlation between H_2O and Li seems unlikely to be primary. We therefore speculate that Li diffusion may have been mediated by the re-equilibration of H_2O; that the activity of Li (a_{Li}) in melt inclusions was controlled by their H_2O contents such that a_{Li} gradients formed at rates controlled by the slower re-equilibration of H_2O. However, further work is required to validate this hypothesis, as well as to investigate the behaviour of Li in plagioclase-hosted inclusions more generally.

7. SYN-ENTRAPMENT MODIFICATION OF MELT INCLUSION COMPOSITIONS

7.1. F enrichment in plagioclase-hosted melt inclusions

Most oceanic glasses have F/Nd values close to $20.1 \pm 5.8(1\sigma)$ (Workman et al., 2006; Shaw et al., 2010; Le Voyer et al., 2015), though values of up to 45.4 have been reported from Macquarie Island (Shimizu et al., 2015). Matrix glasses and olivine-hosted melt inclusions from the 10 ka Grímsvötn tephra series thus define a mean F/Nd value towards the lower end of the oceanic basalts range ($15.0 \pm 2.1(1\sigma)$; Fig. 7c). However, primitive plagioclase-hosted melt inclusions from the tephra have F/Nd values that are well above any previously reported values from primitive basalts (mean = $111.4 \pm 30.1(1\sigma)$). Moreover, F does not correlate with any element in the inclusion suite apart from Al (Supplementary Fig. 3;
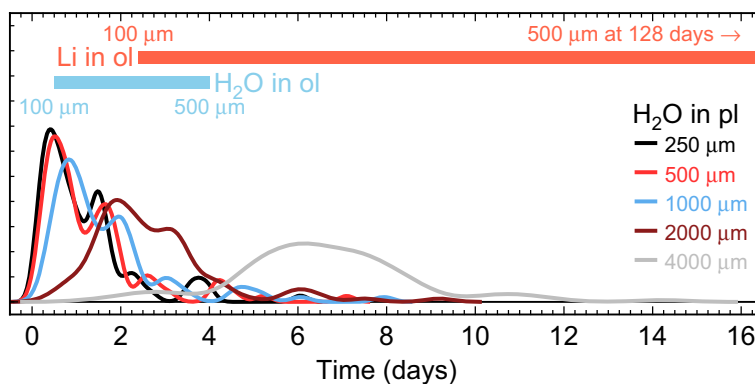

Fig. 9. Plot summarising melt inclusion re-equilibration timescales calculated based on the exchange of H_2O and Li through olivine hosts and H_2O through plagioclase hosts. Coloured lines show kernel density estimates (KDEs) of H_2O re-equilibration timescales in plagioclase-hosted melt inclusions calculated for a range of macrocryst radii (250–4000 μm). The blue bar shows the range of timescales calculated for complete H_2O re-equilibration in melt inclusions hosted in olivine macrocrysts of realistic radii (100–500 μm); these represent minimum re-equilibration timescales. The pale red bar shows the range of timescales calculated for no detectable Li re-equilibration to occur in olivine-hosted melt inclusion with the same host properties; these represent maximum re-equilibration timescales. All calculations assumed that the primitive melt inclusions re-equilibrated with a melt composition identical to the matrix glass with $H_2O/Ce = 180$ at 1140 °C (Neave et al., 2015). (For interpretation of the references to colour in this figure legend, the reader is referred to the web version of this article.)

$r = 0.39; p < 0.01$), which suggests that its enrichment was neither primary nor related to the post-entrapment processes discussed above.

Although open system behaviour of F has been proposed to explain features in some olivine-hosted melt inclusion datasets (Portnyagin et al., 2008; Koleszar et al., 2009), we consider post-entrapment re-equilibration to be an unlikely cause of high F/Nd. This is because the F content of almost all plagioclase-hosted inclusions (PEC-corrected mean = $705 \pm 138 (1\sigma)$ ppm) exceeds that of their carrier liquid ($362 \pm 40 (1\sigma)$ ppm). Assuming that F concentration recapitulates F activity, primitive melt inclusions would thus have to have re-equilibrated with melts that were either more enriched or more evolved than the matrix glasses in order to have acquired their elevated F contents (e.g. transitional basalts or basaltic andesites; Moune et al., 2007; Moune et al., 2012). However, no such interactions are recorded in the tephra's petrology.

Diffusive pile-up of slow-diffusing species against inclusion walls or rapidly growing crystal faces could also generate apparent halogen enrichments in melt inclusions (Baker et al., 2005; Newcombe et al., 2014), but can be discounted in this case because the enrichment in F is not matched by enrichments in more slowly diffusing elements such as Cl, S and Zr (Alletti et al., 2007; Zhang et al., 2010; Behrens and Stelling, 2011). Furthermore, while hydrothermal fluids represent a potential source of halogen contamination, they generally mobilise Cl and alkalis more easily than F, and thus cannot account for the selective enrichment of F (Floyd and Fuge, 1982): neither Cl nor the alkalis are anomalously abundant in primitive inclusions.

7.2. Plagioclase-hosted melt inclusion formation and F enrichment

HFSE depletions in plagioclase-hosted melt inclusions from MORBs are thought to reflect the formation of inclusions by dissolution-crystallisation processes, whereby melt channels formed by resorption partially re-equilibrate with their surrounding melts before being sealed as inclusions (Michael et al., 2002). Although the channelised dissolution of high-anorthite plagioclase remains to be observed in experiments on natural basalts (Kohut and Nielsen, 2003; Kohut and Nielsen, 2004), it has been reported in experiments on the Di–Ab–An–H_2O system (Nakamura and Shimakita, 1998). Moreover, high-anorthite plagioclase-hosted melt inclusions have been formed experimentally within a matter of hours by isothermally annealing hopper and dendritic growths formed during preceding periods of high undercooling, demonstrating that inclusions can seal rapidly (Kohut and Nielsen, 2004).

With these observations in mind, we propose that plagioclase-hosted melt inclusions from the 10 ka Grímsvötn tephra serieswere formed by dissolution-crystallization processes in the following manner. Firstly, we suggest that high-anorthite plagioclase macrocrysts crystallised from high-Ca/Na primitive melts similar to those erupted at Borgarhraun in north Iceland (Maclennan et al., 2003; Neave et al., 2013): matrix glasses

from Borgarhraun are in equilibrium with An$_{86}$ according to the model of Namur et al. (2012). Resorption and channelised dissolution of these macrocrysts may have then taken place after they interacted with lower Ca/Na or hotter melts in which high-anothite plagioclase was unstable (Fig. 9; Neave et al., 2015); there is abundant evidence for the supply of suitably diverse melts to the base of the Icelandic plumbing systems (e.g., Gurenko and Chaussidon, 1995; Maclennan, 2008; Shorttle and Maclennan, 2011). Assuming minimal stirring, perhaps as a result of resorption taking place within a crystal mush (Ridley et al., 2006), the composition of melt pools and channels around and inside resorbing grains would have approached that of dissolved plagioclase, i.e., would have been Al-rich but HFSE-poor (e.g., Yu et al., 2016). Because of the HFSE depletions present in a number of plagioclase-hosted inclusions (Fig. 3; Michael et al., 2002; Neave et al., 2015), we thus propose that at least some inclusions were then trapped from these initially Al-rich and Zr-poor melt pools before they had fully dissipated: HFSEs diffuse ~2.5 times more slowly than REEs and most major elements at the conditions relevant for inclusion formation (~1200 °C; Zhang et al., 2010). It is at this stage of inclusion entrapment from Al-rich melts we suggest that F enrichment took place.

Although the solubility of F in basaltic melts has not been studied extensively, experiments in aluminosilicate model systems indicate that F solubility, i.e., when F activity (a_F) = 1, depends strongly on melt Al/(Al + Si). That is, F is much more soluble in high-Al/(Al + Si) melts as a consequence of F dissolving into aluminosilicate melts by complexing with Al (Mysen et al., 2004; Dalou and Mysen, 2015; Dalou et al., 2015). F solubility is thus likely to have been much higher in any Al-rich melts bathing resorbing plagioclase grains than in the surrounding basalts: An$_{90}$ plagioclase has an Al/(Al + Si) value of ~0.48, whereas primitive Icelandic basalts and the two primitive olivine-hosted melt inclusions from the tephra have Al/(Al + Si) values of ~0.26. This higher solubility would have plausibly resulted in a correspondingly lower a_F at any given F concentration, resulting in the accumulation of F around dissolving grains by uphill diffusion, a process by which a species diffuses up a concentration gradient whilst diffusing down an activity gradient. Crucially, the diffusion of F in basaltic melts at 1200 °C is around six times faster than the diffusion of Al, meaning that F could have diffused into Al-rich regions before they dissipated (Alletti et al., 2007; Zhang et al., 2010), with the degree of F enrichment mediated by the concentration of Al. Furthermore, the location of inclusions within entirely high-anorthite plagioclase cores suggests that the melts immediately surrounding previously resorped grains were still Al-rich at the time of entrapment: if the Al had dispersed, then the inclusions would have been trapped within lower anorthite plagioclase. Thus, the discrepancy between the ~26 vol.% of PEC required to achieve inclusion-host equilibrium and the ~16 vol.% of PEC required to bring melt inclusions into equilibrium with Icelandic glasses could potentially be accounted for by the syn-entrapment crystallisation of

high-anorthite plagioclase acting to reverse much of the preceding dissolution.

Our proposed mechanism of inclusion formation thus predicts that F and Al would correlate negatively with the degree of HFSE depletion, that is, with Zr or Zr/Nd. Unfortunately, no such correlations are observed, though we note that F and Al do correlate with each other ($r = 0.39; p < 0.01$). However, such elemental decoupling is perhaps unsurprising given that Al, F and the HFSEs diffuse at different rates ($D_{Al} < D_{HFSEs} < D_F$; Alletti et al., 2007; Zhang et al., 2010). Furthermore, variability in ITE ratios robust to diffusive fractionation (e.g., La/Yb; Fig. 3c) and poor correlations between measures of HFSE depletion and ITE enrichment (e.g., Zr/Nd versus La/Yb; $r = -0.34; p > 0.1$) indicate that dissolution was driven by compositionally heterogeneous melts and that signals of primary melt variability are dissociated from those of diffusive re-equilibration. Additional support for a dissolution-crystallisation inclusion formation mechanism concerns its ability to simultaneously account for the inclusions' most anomalous features. If HFSE depletion and F enrichment were primary, then myriad exotic melts, for which there are no geological precedents, would need to be invoked.

8. PRE-ENTRAPMENT SIGNALS IN MELT INCLUSION COMPOSITIONS

8.1. S-rich primitive melts

Sulphide-undersaturated MORB glasses are thought to have S/Dy values of 225 ± 49 (Saal et al., 2002), though primary S/Dy may vary as a function of incompatible trace element enrichment (Shimizu et al., 2015). Primitive plagioclase-hosted melt inclusions from the 10 ka Grímsvötn tephra series have a mean S/Dy value of $303 \pm 72(1\sigma)$ that is similar to values from some OIBs and plume-influenced MORBs (Fig. 3e; Workman et al., 2006; Koleszar et al., 2009; Le Voyer et al., 2015). Despite the large uncertainty in S/Dy values inherited from imprecise Dy analyses, S and Dy correlate somewhat ($r = 0.32; p < 0.01$), suggesting that primitive plagioclase-hosted melt inclusions could have been sulphide undersaturated and the time of entrapment.

Conversely, a stronger correlation between S and FeO$_T$ ($r = 0.61; p < 0.01$) would suggest that sulphides could play a role in buffering melt inclusion S contents (Fig. 6b): under the reducing conditions that prevail during oceanic basalt petrogenesis, melt FeO$_T$ exerts a dominant control on the S content of melts at sulphide saturation (SCSS; Li and Naldrett, 1993; O'Neill and Mavrogenes, 2002). However, current SCSS models are equivocal on the state of sulphide saturation in our primitive melt inclusions: assuming a conservative 5% uncertainty in ln(SCSS) values from the model of Fortin et al. (2015) to PEC-corrected primitive melt inclusions at 1200 °C and 3 kbar returns a possible SCSS range of 879–1973 ppm. A mean S/Dy value of $303 \pm 72(1\sigma)$ nonetheless places a minimum bound on primary S/Dy values that is comparable with the highest values reported from oceanic basalts to date.

8.2. Cl and B signals from the mantle

Cl/K values in pristine MORB glasses lie mainly within the 0.01–0.08 range (Michael and Cornell, 1998), though values from the Mid-Atlantic Ridge are often higher (0.05–0.13; Michael and Cornell, 1998; Le Voyer et al., 2015). Matrix glasses and PEC–corrected primitive melt inclusions from the 10 ka Grímsvötn tephra series have mean Cl/K values within the range of typical MORB glasses, but lower than most glasses from the Mid-Atlantic Ridge ($0.050 \pm 0.005(1\sigma)$ and $0.065 \pm 0.014(1\sigma)$ ppm respectively; Fig. 7d). Cl correlates with K in both matrix glasses and primitive inclusions ($r = 0.77$ and 0.55 respectively; $p < 0.01$ in both cases), suggesting that Cl behaved incompatibly during the course of magmatic evolution and that a Cl/K value of 0.050–0.065 is probably primary; Cl was not fractionated by syn- or post-entrapment processes, which is consistent with Cl having a different solution mechanism from F (Dalou et al., 2015).

B correlates most strongly with highly incompatible Ce in primitive melt inclusions ($r = 0.67; p < 0.01$) but with slightly less incompatible elements such as Zr ($r = 0.60; p \sim 0.07$) in matrix glasses. This change in behaviour is consistent with a change in B's bulk solid–liquid partition coefficient from ~0.006 during mantle melting (recorded by primitive melt inclusions) to ~0.07 during low pressure fractional crystallisation (recorded by matrix glasses; Ryan and Langmuir, 1993). B thus appears to have been unaffected by syn- and post-entrapment processes.

9. THE FIDELITY OF PLAGIOCLASE-HOSTED MELT INCLUSION VOLATILE RECORDS

Volatiles in primitive plagioclase-hosted melt inclusions from the 10 ka Grímsvötn tephra series preserve a range of pre-, syn- and post-entrapment signals (Fig. 10). For example, the correlated variability in Cl, B and ITEs is consistent with the entrapment of initially heterogeneous primary melts that have experienced various degrees of mixing; variability in Cl and B is primary in origin. Furthermore, while it is unclear whether inclusions were sulphide-saturated at the time of formation, high S/Dy values in primitive melt inclusions indicate that Icelandic primary melts may be S-rich in comparison with most oceanic basalts.

In contrast, F was probably fractionated by dissolution-crystallisation processes implicated in primitive plagioclase-hosted melt inclusion formation by the presence HFSE depletions in some inclusions. Namely, we propose that plagioclase-hosted inclusions formed by the entrapment of initially Al-rich melts generated by the variable re-equilibration of dissolved plagioclase with recharging melts and whose Al-rich nature facilitated F enrichment by uphill diffusion. While there are few published analyses of F in plagioclase-hosted melt inclusions from oceanic basalts for comparison, we suggest that F enrichment could occur in any system where plagioclase dissolution played a role in inclusion formation.

Apart from PEC, which would have initially acted to concentrate all volatile and incompatible elements, melt
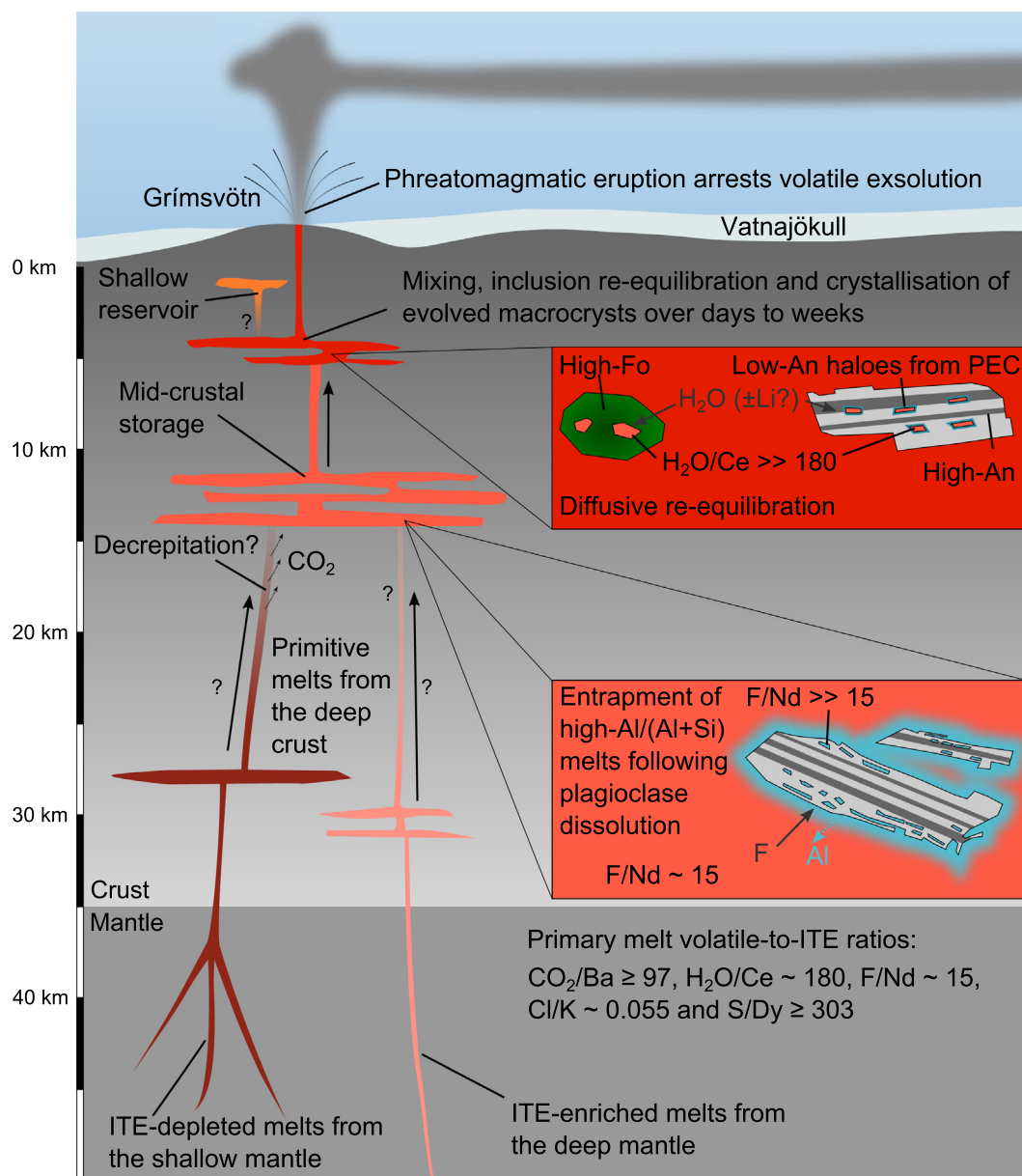
Fig. 10. Figure summarising the magmatic processes recorded by volatile and light lithophile elements in matrix glasses and melt inclusions from the 10 ka Grímsvötn tephra series.

inclusion decrepitation was probably the first post-entrapment process to modify inclusion compositions. We suggest that the almost uniformly low CO_2 content of primitive melt inclusions reflects decrepitation as a result of PEC and decompression during ascent; a single inclusion with $CO_2/Ba \sim 97$ may be primary.

High H_2O/Ce values in primitive plagioclase-hosted melt inclusions suggest they became overhydrated by partially re-equilibrating with their more evolved and hydrous carrier liquids *en route* to the surface. Diffusion calculations suggest that primitive macrocrysts resided in evolved carrier liquids for a few days before eruption, a value comparable with macrocryst entrainment timescales reported from petrologically similar systems. The H_2O content of

plagioclase-hosted melt inclusions in basaltic systems may thus be modified within hours of host macrocrysts being transferred between melts of variable a_{H_2O}. A strong correlation between H_2O and Li in plagioclase-hosted inclusions suggests that H_2O-mediated diffusive exchange of Li through plagioclase may have occurred as well.

Despite the paucity of primary signals in our plagioclase-hosted inclusion dataset, the diverse behaviour of volatiles nevertheless presents numerous opportunities for investigating magma evolution. For example, F enrichments lend further credence to previously suggested models of primitive plagioclase-hosted inclusion formation by dissolution-crystallisation processes. Furthermore, the slower diffusion of H^+ though plagioclase than through oli-

vine represents a potential chronometric tool for investigating mixing and transport processes over the days-to-weeks timescale crucial for understanding pre-eruptive processes. Thus, while primary melt volatile contents can remain elusive in both olivine- and plagioclase-hosted melt inclusion archives, primitive plagioclase-hosted inclusions contain distinct records that complement and enrich those from matrix glasses and olivine-hosted melt inclusions.

ACKNOWLEDGEMENTS

APPENDIX A. SUPPLEMENTARY DATA

Supplementary data associated with this article can be found, in the online version, at http://dx.doi.org/10.1016/j.gca.2017.02.009.

REFERENCES

Adams D. T., Nielsen R. L., Kent A. J. R. and Tepley F. J. (2011) Origin of minor and trace element compositional diversity in anorthitic feldspar phenocrysts and melt inclusions from the Juan de Fuca Ridge. *Geochem. Geophys. Geosyst.* **12**, 1–18. http://dx.doi.org/10.1029/2011GC003778.

Alletti M., Baker D. R. and Freda C. (2007) Halogen diffusion in a basaltic melt. *Geochim. Cosmochim. Acta* **71**, 3570–3580. http://dx.doi.org/10.1016/j.gca.2007.04.018.

Anderson A. T. and Brown G. G. (1993) CO_2 contents and formation pressures of some Kilauean melt inclusions. *Am. Mineral.* **78**, 794–803.

Baker D. R. (2008) The fidelity of melt inclusions as records of melt composition. *Contrib. Miner. Petrol.* **156**, 377–395. http://dx.doi.org/10.1007/s00410-008-0291-3.

Baker D. R., Freda C., Brooker R. A. and Scarlato P. (2005) Volatile diffusion in silicate melts and its effects on melt inclusions. *Ann. Geophys.* **48**, 699–717.

Bédard J. H. (2005) Partitioning coefficients between olivine and silicate melts. *Lithos* **83**, 394–419. http://dx.doi.org/10.1016/j.lithos.2005.03.011.

Behrens H. and Stelling J. (2011) Diffusion and redox reactions of sulfur in silicate melts. *Rev. Mineral. Geochem.* **73**, 79–111. http://dx.doi.org/10.2138/rmg.2011.73.4.

Blundy J. D. and Cashman K. V. (2005) Rapid decompression-driven crystallization recorded by melt inclusions from Mount St. Helens volcano. *Helens Volcano Geol.* **33**, 793–796. http://dx.doi.org/10.1130/G21668.1.

Bodnar, R. J. (2003). Reequilibration of fluid inclusions. In Fluid inclusions: Analysis and interpretation. Mineralogical Association of Canada, Short Course 32, Chapter 8. pp. 213–230.

Bramham-Law C. W. F., Theuerkauf M., Lane C. S. and Mangerud J. (2013) New findings regarding the Saksunarvatn

Ash in Germany. *J. Quat. Sci.* **28**, 248–257. http://dx.doi.org/10.1002/jqs.2615.

Brenan J. M., Neroda E., Lundstrom C. C., Shaw H. F., Ryerson F. J. and Phinney D. L. (1998) Behaviour of boron, beryllium, and lithium during melting and crystallization: constraints from mineral-melt partitioning experiments. *Geochim. Cosmochim. Acta* **62**, 2129–2141. http://dx.doi.org/10.1016/S0016-7037(98)00131-8.

Bucholz C. E., Gaetani G. A., Behn M. D. and Shimizu N. (2013) Post-entrapment modification of volatiles and oxygen fugacity in olivine-hosted melt inclusions. *Earth Planet. Sci. Lett.* **374**, 145–155. http://dx.doi.org/10.1016/j.epsl.2013.05.033.

Burgisser A., Alletti M. and Scaillet B. (2015) Simulating the behavior of volatiles belonging to the C-O-H-S system in silicate melts under magmatic conditions with the software D-Compress. *Comput. Geosci.* **79**, 1–14. http://dx.doi.org/10.1016/j.cageo.2015.03.002.

Burnham C. W. (1979) The importance of volatile constituents. In *Evolution of the Igneous Rocks: Fiftieth Anniversary Perspectives* (ed. H. J. Yoder). Princeton University Press, Princeton, pp. 439–482, Chapter 16.

Carroll M. R. and Webster J. D. (1994) Solubilities of sulfur, noble gases, nitrogen, chlorine, and fluorine in magmas. *Rev. Mineral. Geochem.* **30**, 231–280.

Cassidy M., Castro J. M., Helo C., Troll V. R., Deegan F. M., Muir D., Neave D. A. and Mueller S. P. (2016) Volatile dilution during magma injections and implications for volcano explosivity. *Geology* **44**, 1027–1030. http://dx.doi.org/10.1130/G38411.1.

Chen Y., Provost A., Schiano P. and Cluzel N. (2013) Magma ascent rate and initial water concentration inferred from diffusive water loss from olivine-hosted melt inclusions. *Contrib. Miner. Petrol.* **165**, 525–541. http://dx.doi.org/10.1007/s00410-012-0821-x.

Cottrell E., Spiegelman M. and Langmuir C. H. (2002) Consequences of diffusive reequilibration for the interpretation of melt inclusions. *Geochem. Geophys. Geosyst.* **3**, 1–26. http://dx.doi.org/10.1029/2001GC000205.

Dalou C., Koga K. T., Shimizu N., Boulon J. and Devidal J. L. (2012) Experimental determination of F and Cl partitioning between lherzolite and basaltic melt. *Contrib. Miner. Petrol.* **163**, 591–609. http://dx.doi.org/10.1007/s00410-011-0688-2.

Dalou C., Le Losq C., Mysen B. O. and Cody G. D. (2015) Solubility and solution mechanisms of chlorine and fluorine in aluminosilicate melts at high pressure and high temperature. *Am. Mineral.* **100**, 2272–2283. http://dx.doi.org/10.2138/am-2015-5201.

Dalou C. and Mysen B. O. (2015) The effect of H_2O on F and Cl solubility and solution mechanisms of in aluminosilicate melts at high pressure and high temperature. *Am. Mineral.* **100**, 633–643. http://dx.doi.org/10.2138/am-2015-4814.

Danyushevsky L. V. and Plechov P. (2011) Petrolog 3: integrated software for modeling crystallization processes. *Geochem. Geophys. Geosyst.* **12**. http://dx.doi.org/10.1029/2011GC003516.

Demouchy S. and Mackwell S. (2006) Mechanisms of hydrogen incorporation and diffusion in iron-bearing olivine. *Phys. Chem. Miner.* **33**, 347–355. http://dx.doi.org/10.1007/s00269-006-0081-2.

Dixon J. E. and Stolper E. M. (1995) An experimental study of water and carbon dioxide solubilities in mid-ocean ridge basaltic liquids. Part II. Applications to degassing. *J. Petrol.* **36**, 1633–1646.

Dohmen R. and Blundy J. D. (2014) A predictive thermodynamic model for element partitioning between plagioclase and melt.

Am. J. Sci. **314**, 1319–1372. http://dx.doi.org/10.2475/09.2014.04.

Dohmen R., Kasemann S. A., Coogan L. and Chakraborty S. (2010) Diffusion of Li in olivine. Part I: experimental observations and a multi species diffusion model. *Geochim. Cosmochim. Acta* **74**, 274–292. http://dx.doi.org/10.1016/j.gca.2009.10.016.

Duncan R. A. and Green D. H. (1987) The genesis of refractory melts in the formation of oceanic crust. *Contrib. Miner. Petrol.* **96**, 326–342. http://dx.doi.org/10.1007/BF00371252.

Esposito R., Lamadrid H. M., Redi D., Steele-Macinnis M. J., Bodnar R. J., Manning C. E., De Vivo B., Cannatelli C. and Lima A. (2016) Detection of liquid H_2O in vapor bubbles in reheated melt inclusions: implications for magmatic fluid composition and volatile budgets of magmas? *Am. Mineral.* **101**, 1691–1695.

Faure F. and Schiano P. (2005) Experimental investigation of equilibration conditions during forsterite growth and melt inclusion formation. *Earth Planet. Sci. Lett.* **236**, 882–898. http://dx.doi.org/10.1016/j.epsl.2005.04.050.

Flower M. F. J. (1980) Accumulation of calcic plagioclase in ocean-ridge tholeiite: an indication of spreading rate? *Nature* **287**, 530–532. http://dx.doi.org/10.1038/287530a0.

Floyd P. A. and Fuge R. (1982) Primary and secondary alkali and halogen element distribution in Iceland Research Drilling Project basalts from eastern Iceland. *J. Geophys. Res.* **87**, 6477–6488. http://dx.doi.org/10.1029/JB087iB08p06477.

Font L., Murton B. J., Roberts S. and Tindle A. G. (2007) Variations in melt productivity and melting conditions along SWIR (70°E–49°E): evidence from olivine-hosted and plagioclase-hosted melt inclusions. *J. Petrol.* **48**, 1471–1494. http://dx.doi.org/10.1093/petrology/egm026.

Ford C. E., Russell D. G., Craven J. A. and Fisk M. R. (1983) Olivine-liquid equilibria: temperature, pressure and composition dependence of the crystal/liquid cation partition coefficients for Mg, Fe^{2+}, Ca and Mn. *J. Petrol.* **24**, 256–265.

Fortin M. A., Riddle J., Desjardins-Langlais Y. and Baker D. R. (2015) The effect of water on the sulfur concentration at sulfide saturation (SCSS) in natural melts. *Geochim. Cosmochim. Acta* **160**, 100–116. http://dx.doi.org/10.1016/j.gca.2015.03.022.

Gaetani G. A., O'Leary J. A., Shimizu N., Bucholz C. E. and Newville M. (2012) Rapid reequilibration of H_2O and oxygen fugacity in olivine-hosted melt inclusions. *Geology* **40**, 915–918. http://dx.doi.org/10.1130/G32992.1.

Giletti B. J. and Shanahan T. M. (1997) Alkali diffusion in plagioclase feldspar. *Chem. Geol.* **139**, 3–20. http://dx.doi.org/10.1016/S0009-2541(97)00026-0.

Grönvold K., Óskarsson N., Johnsen S. J., Clausen H. B., Hammer C. U., Bond G. and Bard E. (1995) Ash layers from Iceland in the Greenland GRIP ice core correlated with oceanic and land sediments. *Earth Planet. Sci. Lett.* **135**, 149–155. http://dx.doi.org/10.1016/0012-821X(95)00145-3.

Guggino S. (2012) *Fluorine Partitioning Between Nominally Anhydrous Minerals (Olivine, Clinopyroxene, and Plagioclase) and Silicate Melt Using Secondary Ion Mass Spectrometry and Newly Synthesized Basaltic Fluorine Microanalytical Glass Standards* (Ph.D. thesis). Arizona State University.

Gurenko A. A. and Chaussidon M. (1995) Enriched and depleted primitive melts included in olivine from Icelandic tholeiites: origin by continuous melting of a single mantle column. *Geochim. Cosmochim. Acta* **59**, 2905–2917. http://dx.doi.org/10.1016/0016-7037(95)00184-0.

Halldórsson S. A., Óskarsson N., Sigurdsson G., Sverrisdottir G. and Steinthórsson S. (2008) Isotopic-heterogeneity of the Thjorsa lava-Implications for mantle sources and crustal processes within the Eastern Rift Zone, Iceland. *Chem. Geol.* **255**, 305–316. http://dx.doi.org/10.1016/j.chemgeo.2008.06.050.

Hamada M., Kawamoto T., Takahashi E. and Fujii T. (2011) Polybaric degassing of island arc low-K tholeiitic basalt magma recorded by OH concentrations in Ca-rich plagioclase. *Earth Planet. Sci. Lett.* **308**, 259–266. http://dx.doi.org/10.1016/j.epsl.2011.06.005.

Hamada M., Ushioda M., Fujii T. and Takahashi E. (2013) Hydrogen concentration in plagioclase as a hygrometer of arc basaltic melts: approaches from melt inclusion analyses and hydrous melting experiments. *Earth Planet. Sci. Lett.* **365**, 253–262. http://dx.doi.org/10.1016/j.epsl.2013.01.026.

Hansen H. and Grönvold K. (2000) Plagioclase ultraphyric basalts in Iceland: the mush of the rift. *J. Volcanol. Geoth. Res.* **98**, 1–32. http://dx.doi.org/10.1016/S0377-0273(99)00189-4.

Hartley M. E., Maclennan J., Edmonds M. and Thordarson T. (2014) Reconstructing the deep CO_2 degassing behaviour of large basaltic fissure eruptions. *Earth Planet. Sci. Lett.* **393**, 120–131. http://dx.doi.org/10.1016/j.epsl.2014.02.031.

Hartley M. E., Morgan D. J., Maclennan J., Edmonds M. and Thordarson T. (2016) Tracking timescales of short-term precursors to large basaltic fissure eruptions through Fe-Mg diffusion in olivine. *Earth Planet. Sci. Lett.* **439**, 58–70. http://dx.doi.org/10.1016/j.epsl.2016.01.018.

Hartley M. E., Neave D. A., Maclennan J., Edmonds M. and Thordarson T. (2015) Diffusive over-hydration of olivine-hosted melt inclusions. *Earth Planet. Sci. Lett.* **425**, 168–178. http://dx.doi.org/10.1016/j.epsl.2015.06.008.

Hauri E. H., Gaetani G. A. and Green T. H. (2006) Partitioning of water during melting of the Earth's upper mantle at H_2O-undersaturated conditions. *Earth Planet. Sci. Lett.* **248**, 715–734. http://dx.doi.org/10.1016/j.epsl.2006.06.014.

Helo C., Longpré M. A., Shimizu N., Clague D. A. and Stix J. (2011) Explosive eruptions at mid-ocean ridges driven by CO_2-rich magmas. *Nat. Geosci.* **4**, 260–263. http://dx.doi.org/10.1038/ngeo1104.

Herzberg C. and O'Hara M. J. (2002) Plume-associated ultramafic magmas of phanerozoic age. *J. Petrol.* **43**, 1857–1883. http://dx.doi.org/10.1093/petrology/43.10.1857.

Hinton R. (1990) Ion microprobe trace-element analysis of silicates: measurement of multi-element glasses. *Chem. Geol.* **83**, 11–25. http://dx.doi.org/10.1016/0009-2541(90)90136-U.

Jarosewich E., Nelen J. A. and Norberg J. A. (1980) Reference samples for electron microprobe analysis. *Geostand. Newslett.* **4**, 43–47.

Jenner F. E. and O'Neill H. S. C. (2012) Analysis of 60 elements in 616 ocean floor basaltic glasses. *Geochem. Geophys. Geosyst.* **13**, 1–11. http://dx.doi.org/10.1029/2011GC004009.

Jennings A., Thordarson T., Zalzal K., Stoner J., Hayward C. L., Geirsdottir A. and Miller G. (2014) Holocene tephra from Iceland and Alaska in SE Greenland Shelf Sediments. *Geol. Soc. London* **398**, 157–193. http://dx.doi.org/10.1144/SP398.6, Special Publications.

Jochum K. P., Stoll B., Herwig K., Willbold M., Hofmann A. W., Amini M., Aarburg S., Abouchami W., Hellebrand E., Mocek B., Raczek I., Stracke A., Alard O., Bouman C., Becker S., Dücking M., Brätz H., Klemd R., de Bruin D., Canil D., Cornell D., de Hoog C. J., Dalpé C., Danyushevsky L. V., Eisenhauer A., Gao Y., Snow J. E., Groschopf N., Günther D., Latkoczy C., Guillong M., Hauri E. H., Höfer H. E., Lahaye Y., Horz K., Jacob D. E., Kasemann S. A., Kent A. J. R., Ludwig T., Zack T., Mason P. R. D., Meixner A., Rosner M., Misawa K., Nash B. P., Pfänder J., Premo W. R., Sun W. D., Tiepolo M., Vannucci R., Vennemann T., Wayne D. and Woodhead J. D. (2006) MPI-DING reference glasses for in situ microanalysis: new reference values for element concentrations and isotope ratios. *Geochem. Geophys. Geosyst.* **7**, 1–44. http://dx.doi.org/10.1029/2005GC001060.

Jochum K. P., Weis U., Stoll B., Kuzmin D., Yang Q., Raczek I., Jacob D. E., Stracke A., Birbaum K., Frick D. A., Günther D. and Enzweiler J. (2011) Determination of reference values for NIST SRM 610–617 glasses following ISO guidelines. *Geostand. Geoanal. Res.* **35**, 397–429. http://dx.doi.org/10.1111/j.1751-908X.2011.00120.x.

Jóhannsdóttir G. E. (2007) *Mid Holocene to late glacial tephrochronology in west Iceland as revealed in three lacustrine environments* (M.S. thesis). University of Iceland.

Jóhannsdóttir G. E., Thordarson T., Geirsdóttir A. and Larsen G. (2005) The widespread ~10 ka Saksunarvatn tephra: a product of three large basaltic phreatoplinian eruptions? *Geophys. Res. Abstr.* **7**, 05991.

Johnson E. A. (2005). Magmatic water contents recorded by hydroxyl concentrations in plagioclase phenocrysts from Mount St. Helens, 1980–1981. Goldschmidt Conference Abstracts 2005 A743.

Johnson E. A. and Rossman G. R. (2013) The diffusion behavior of hydrogen in plagioclase feldspar at 800–1000°C: implications for re-equilibration of hydroxyl in volcanic phenocrysts. *Am. Mineral.* **98**, 1779–1787. http://dx.doi.org/10.2138/am.2013.4521.

Kent A. J. R. (2008) Melt Inclusions in basaltic and related volcanic rocks. *Rev. Mineral. Geochem.* **69**, 273–331. http://dx.doi.org/10.2138/rmg.2008.69.8.

van den Kerkhof A. M. and Hein U. F. (2001) Fluid inclusion petrography. *Lithos* **55**, 27–47. http://dx.doi.org/10.1016/S0024-4937(00)00037-2.

Kohut E. J. and Nielsen R. L. (2003) Low-pressure phase equilibria of anhydrous anorthite-bearing mafic magmas. *Geochem. Geophys. Geosyst.* **4**, 1–27. http://dx.doi.org/10.1029/2002GC000451.

Kohut E. J. and Nielsen R. L. (2004) Melt inclusion formation mechanisms and compositional effects in high – an feldspar and high-Fo olivine in anhydrous mafic silicate liquids. *Contrib. Miner. Petrol.* **147**, 684–704. http://dx.doi.org/10.1007/s00410-004-0576-0.

Koleszar A. M., Saal A. E., Hauri E. H., Nagle A. N., Liang Y. and Kurz M. D. (2009) The volatile contents of the Galapagos plume; evidence for H_2O and F open system behavior in melt inclusions. *Earth Planet. Sci. Lett.* **287**, 442–452. http://dx.doi.org/10.1016/j.epsl.2009.08.029.

Kress V. C. and Ghiorso M. S. (2004) Thermodynamic modeling of post-entrapment crystallization in igneous phases. *J. Volcanol. Geoth. Res.* **137**, 247–260. http://dx.doi.org/10.1016/j.jvolgeores.2004.05.012.

Lange A. E., Nielsen R. L., Tepley F. J. and Kent A. J. R. (2013) The petrogenesis of plagioclase-phyric basalts at mid-ocean ridges. *Geochem. Geophys. Geosyst.* **14**, 3282–3296. http://dx.doi.org/10.1002/ggge.20207.

Langmuir C. H., Klein E. M. and Plank T. (1992) Mantle flow and melt generation at mid-ocean ridges. *Geophys. Monogr. Ser.* **71**, 183–280. http://dx.doi.org/10.1029/GM071.

Le Voyer M., Asimow P. D., Mosenfelder J. L., Guan Y., Wallace P. J., Schiano P., Stolper E. M. and Eiler J. M. (2014) Zonation of H_2O and F concentrations around melt inclusions in olivines. *J. Petrol.* **55**, 685–707. http://dx.doi.org/10.1093/petrology/egu003.

Le Voyer M., Cottrell E., Kelley K. A., Brounce M. and Hauri E. H. (2015) The effect of primary versus secondary processes on the volatile content of MORB glasses: an example from the equatorial Mid-Atlantic Ridge (5°N–3°S). *J. Geophys. Res.* **120**, 125–144. http://dx.doi.org/10.1002/2014JB011160.

Li C. and Naldrett A. J. (1993) Sulfide capacity of magma: a quantitative model and its application to the formation of sulfide ores at Sudbury, Ontario. *Econ. Geol.* **88**, 1253–1260. http://dx.doi.org/10.2113/gsecongeo.88.5.1253.

Lloyd A. S., Plank T., Ruprecht P., Hauri E. H. and Rose W. (2013) Volatile loss from melt inclusions in pyroclasts of differing sizes. *Contrib. Miner. Petrol.* **165**, 129–153. http://dx.doi.org/10.1007/s00410-012-0800-2.

Lowenstern J. B. (1995). Applications of silicate-melt inclusions to the study of magmatic volatiles. In Magmas, Fluids and Ore Deposits. Mineralogical Association of Canada Short Course. Mineralogical Association of Canada Short Course 23. Vol. 23. pp. 71–99 (Chapter 4).

Maclennan J. (2008) Concurrent mixing and cooling of melts under Iceland. *J. Petrol.* **49**, 1931–1953. http://dx.doi.org/10.1093/petrology/egn052.

Maclennan J. (2017) Bubble formation and decrepitation control the CO_2 content of olivine-hosted melt inclusions. *Geochem. Geophys. Geosyst.*. http://dx.doi.org/10.1002/2016GC006633.

Maclennan J., McKenzie D., Hilton F., Grönvold K. and Shimizu N. (2003) Geochemical variability in a single flow from northern Iceland. *J. Geophys. Res.* **108**, 1–21. http://dx.doi.org/10.1029/2000JB000142.

Mangerud J., Furnes H. and Jóhansen J. (1986) A 9000-year-old ash bed on the Faroe islands. *Quatern. Res.* **26**, 262–265. http://dx.doi.org/10.1016/0033-5894(86)90109-2.

Marks M. A. W., Kendrick M. A., Eby N. G., Zack T. and Wenzel T. (2016) The F, Cl, Br and I contents of reference glasses BHVO-2G, BIR-1G, BCR-2G, GSD-1G, GSE-1G, NIST SRM 610 and NIST SRM 612. *Geostand. Geoanal. Res.* **1–48**. http://dx.doi.org/10.1111/ggr.12128.

Massare D., Métrich N. and Clocchiatti R. (2002) High-temperature experiments on silicate melt inclusions in olivine at 1 atm: inference on temperatures of homogenization and H_2O concentrations. *Chem. Geol.* **183**, 87–98. http://dx.doi.org/10.1016/S0009-2541(01)00373-4.

Métrich N. and Wallace P. J. (2008) Volatile abundances in basaltic magmas and their degassing paths tracked by melt inclusions. *Rev. Mineral. Geochem.* **69**, 363–402. http://dx.doi.org/10.2138/rmg.2008.69.10.

Michael P. J. (1995) Evidence from trace elements and H_2O for regionally distinctive sources of depleted MORB: implications for evolution of the depleted mantle. *Earth Planet. Sci. Lett.* **131**, 301–320. http://dx.doi.org/10.1180/minmag.1994.58A.2.52.

Michael P. J. and Cornell W. C. (1998) Influence of spreading rate and magma supply on crystallization and assimilation beneath mid-ocean ridges: evidence from chlorine and major element chemistry of mid-ocean ridge basalts. *J. Geophys. Res.* **103**, 18325–18356. http://dx.doi.org/10.1029/98JB00791.

Michael P. J. and Graham D. W. (2015) The behavior and concentration of CO_2 in the suboceanic mantle: inferences from undegassed ocean ridge and ocean island basalts. *Lithos* **236–237**, 338–351. http://dx.doi.org/10.1016/j.lithos.2015.08.020.

Michael P. J., McDonough W. F., Nielsen R. L. and Cornell W. C. (2002) Depleted melt inclusions in MORB plagioclase: messages from the mantle or mirages from the magma chamber? *Chem. Geol.* **183**, 43–61. http://dx.doi.org/10.1016/S0009-2541(01)00371-0.

Moore L. R., Gazel E., Tuohy R., Lloyd A. S., Epsosito R., Steele-MacInnis M. J., Hauri E. H., Wallace P. J., Plank T. and Bodnar R. J. (2015) Bubbles matter: an assessment of the contribution of vapor bubbles to melt inclusion volatile budgets. *Am. Mineral.* **100**, 806–823.

Moune S., Sigmarsson O., Schiano P., Thordarson T. and Keiding J. K. (2012) Melt inclusion constraints on the magma source of Eyjafjallajökull 2010 flank eruption. *J. Geophys. Res.* **117**, 1–13. http://dx.doi.org/10.1029/2011JB008718.

Moune S., Sigmarsson O., Thordarson T. and Gauthier P. J. (2007) Recent volatile evolution in the magmatic system of Hekla volcano, Iceland. *Earth Planet. Sci. Lett.* **255**, 373–389. http://dx.doi.org/10.1016/j.epsl.2006.12.024.

Mysen B. O., Cody G. D. and Smith A. (2004) Solubility mechanisms of fluorine in peralkaline and meta-aluminous silicate glasses and in melts to magmatic temperatures. *Geochim. Cosmochim. Acta* **68**, 2745–2769. http://dx.doi.org/10.1016/j.gca.2003.12.015.

Nakamura M. and Shimakita S. (1998) Dissolution origin and syn-entrapment compositional change of melt inclusion in plagioclase. *Earth Planet. Sci. Lett.* **161**, 119–133. http://dx.doi.org/10.1016/S0012-821X(98)00144-7.

Namur O., Charlier B., Toplis M. J. and Vander Auwera J. (2012) Prediction of plagioclase-melt equilibria in anhydrous silicate melts at 1-atm. *Contrib. Miner. Petrol.* **163**, 133–150. http://dx.doi.org/10.1007/s00410-011-0662-z.

Neave D. A., Maclennan J., Edmonds M. and Thordarson T. (2014a) Melt mixing causes negative correlation of trace element enrichment and CO_2 content prior to an Icelandic eruption. *Earth Planet. Sci. Lett.* **400**, 272–283. http://dx.doi.org/10.1016/j.epsl.2014.05.050.

Neave D. A., Maclennan J., Hartley M. E., Edmonds M. and Thordarson T. (2014b) Crystal storage and transfer in basaltic systems: the Skuggafjöll eruption, Iceland. *J. Petrol.* **55**, 2311–2346. http://dx.doi.org/10.1093/petrology/egu058.

Neave D. A., Maclennan J., Thordarson T. and Hartley M. E. (2015) The evolution and storage of primitive melts in the Eastern Volcanic Zone of Iceland: the 10 ka Grímsvötn tephra series (i.e. the Saksunarvatn ash). *Contrib. Miner. Petrol.* **170**, 1–23. http://dx.doi.org/10.1007/s00410-015-1170-3.

Neave D. A., Passmore E., Maclennan J., Fitton J. G. and Thordarson T. (2013) Crystal-melt relationships and the record of deep mixing and crystallization in the AD 1783 Laki eruption, Iceland. *J. Petrol.* **54**, 1661–1690. http://dx.doi.org/10.1093/petrology/egt027.

Neave D. A. and Putirka K. D. (2017) A new clinopyroxene-liquid barometer, and implications for magma storage pressures under Icelandic rift zones. *Am. Mineral.*. http://dx.doi.org/10.2138/am-2017-5968.

Newcombe M. E., Fabbrizio A., Zhang Y., Ma C., Le Voyer M., Guan Y., Eiler J. M., Saal A. E. and Stolper E. M. (2014) Chemical zonation in olivine-hosted melt inclusions. *Contrib. Miner. Petrol.* **168**, 1–26. http://dx.doi.org/10.1007/s00410-014-1030-6.

Nielsen R. L. (2011) The effects of re-homogenization on plagioclase hosted melt inclusions. *Geochem. Geophys. Geosyst.* **12**, 1–16. http://dx.doi.org/10.1029/2011GC003822.

Nielsen R. L., Crum J., Bourgeois R., Hascall K., Forsythe L. M., Fisk M. R. and Christie D. M. (1995) Melt inclusions in high – an plagioclase from the Gorda Ridge: an example of the local diversity of MORB parent magmas. *Contrib. Miner. Petrol.* **122**, 34–50. http://dx.doi.org/10.1180/minmag.1994.58A.2.75.

Nielsen R. L., Michael P. J. and Sours-Page R. (1998) Chemical and physical indicators of compromised melt inclusions. *Geochim. Cosmochim. Acta* **62**, 831–839. http://dx.doi.org/10.1016/S0016-7037(98)00024-6.

O'Hara M. J. (1968) Are ocean floor basalt primary magma? *Nature* **220**, 683–686.

O'Neill H. S. C. and Jenner F. E. (2012) The global pattern of trace-element distributions in ocean floor basalts. *Nature* **491**, 698–704. http://dx.doi.org/10.1038/nature11678.

O'Neill H. S. C. and Mavrogenes J. A. (2002) The sulfide capacity and the sulfur content at sulfide saturation of silicate melts at 1400 °C and 1 bar. *J. Petrol.* **43**, 1049–1087. http://dx.doi.org/10.1093/petrology/43.6.1049.

Panjasawatwong Y., Danyushevsky L. V., Crawford A. J. and Harris K. L. (1995) An experimental study of the effects of melt composition on plagioclase-melt equilibria at 5 and 10 kbar: implications for the origin of magmatic high – an plagioclase. *Contrib. Miner. Petrol.* **118**, 420–432. http://dx.doi.org/10.1007/s004100050024.

Portnyagin M., Almeev R. R., Matveev S. and Holtz F. (2008) Experimental evidence for rapid water exchange between melt inclusions in olivine and host magma. *Earth Planet. Sci. Lett.* **272**, 541–552. http://dx.doi.org/10.1016/j.epsl.2008.05.020.

Qin Z., Lu F. and Anderson A. T. (1992) Diffusive reequilibration of melt and fluid inclusions. *Am. Mineral.* **77**, 565–576.

Ridley I. W., Perfit M. R., Smith M. C. and Fornari D. J. (2006) Magmatic processes in developing oceanic crust revealed in a cumulate xenolith collected at the East Pacific Rise, 9°50'N. *Geochem. Geophys. Geosyst.* **7**, 1–25. http://dx.doi.org/10.1029/2006GC001316.

Roedder E. (1979) Origin and significance of magmatic inclusions. *Bull. Mineral.* **102**, 487–510.

Roedder E. (1984) Fluid inclusions. *Rev. Mineral. Geochem.* **12**, 1–646.

Roeder P. L. and Emslie R. F. (1970) Olivine-liquid equilibrium. *Contrib. Miner. Petrol.* **29**, 275–289. http://dx.doi.org/10.1007/BF00371276.

Rosenthal A., Hauri E. H. and Hirschmann M. M. (2015) Experimental determination of C, F, and H partitioning between mantle minerals and carbonated basalt, CO_2/Ba and CO_2/Nb systematics of partial melting, and the CO_2 contents of basaltic source regions. *Earth Planet. Sci. Lett.* **412**, 77–87. http://dx.doi.org/10.1016/j.epsl.2014.11.044.

Rubin K. H., Sinton J. M., Maclennan J. and Hellebrand E. (2009) Magmatic filtering of mantle compositions at mid-ocean-ridge volcanoes. *Nat. Geosci.* **2**, 321–328. http://dx.doi.org/10.1038/ngeo504.

Ryan J. G. and Langmuir C. H. (1987) The systematics of lithium abundances in young volcanic rocks. *Geochim. Cosmochim. Acta* **51**, 1727–1741. http://dx.doi.org/10.1016/0016-7037(87)90351-6.

Ryan J. G. and Langmuir C. H. (1993) The systematics of boron abundances in young volcanic rocks. *Geochim. Cosmochim. Acta* **57**, 1489–1498. http://dx.doi.org/10.1016/0016-7037(93)90008-K.

Saal A. E., Hauri E. H., Langmuir C. H. and Perfit M. R. (2002) Vapour undersaturation in primitive mid-ocean-ridge basalt and the volatile content of Earth's upper mantle. *Nature* **419**, 451–455. http://dx.doi.org/10.1038/nature01073.

Schiano P. (2003) Primitive mantle magmas recorded as silicate melt inclusions in igneous minerals. *Earth Sci. Rev.* **63**, 121–144. http://dx.doi.org/10.1016/S0012-8252(03)00034-5.

Shaw A. M., Behn M. D., Humphris S. E., Sohn R. A. and Gregg P. M. (2010) Deep pooling of low degree melts and volatile fluxes at the 85°E segment of the Gakkel Ridge: evidence from olivine-hosted melt inclusions and glasses. *Earth Planet. Sci. Lett.* **289**, 311–322. http://dx.doi.org/10.1016/j.epsl.2009.11.018.

Shimizu K., Saal A. E., Myers C. E., Nagel A. N., Hauri E. H., Forsyth D. W., Kamenetsky V. S. and Niu Y. (2015) Two-component mantle melting-mixing model for the generation of mid-ocean ridge basalts: implications for the volatile content of the Pacific upper mantle. *Geochim. Cosmochim. Acta*. http://dx.doi.org/10.1016/j.gca.2015.10.033.

Shishkina T. A., Botcharnikov R. E., Holtz F., Almeev R. R., Jazwa A. M. and Jakubiak A. A. (2014) Compositional and pressure effects on the solubility of H_2O and CO_2 in mafic melts. *Chem. Geol.* **388**, 112–129. http://dx.doi.org/10.1016/j.chemgeo.2014.09.001.

Shorttle O. (2015) Geochemical variability in MORB controlled by concurrent mixing and crystallisation. *Earth Planet. Sci. Lett.* **424**, 1–14. http://dx.doi.org/10.1016/j.epsl.2015.04.035.

Shorttle O. and Maclennan J. (2011) Compositional trends of Icelandic basalts: implications for short-length scale lithological heterogeneity in mantle plumes. *Geochem. Geophys. Geosyst.* **12**, 1–32. http://dx.doi.org/10.1029/2011GC003748.

Shorttle O., Maclennan J. and Jones S. M. (2010) Control of the symmetry of plume-ridge interaction by spreading ridge geometry. *Geochem. Geophys. Geosyst.* **11**, 1–27. http://dx.doi.org/10.1029/2009GC002986.

Shorttle O., Moussallam Y., Hartley M. E., Maclennan J., Edmonds M. and Murton B. J. (2015) Fe-XANES analyses of Reykjanes Ridge basalts: implications for oceanic crust's role in the solid Earth oxygen cycle. *Earth Planet. Sci. Lett.* **427**, 272–285. http://dx.doi.org/10.1016/j.epsl.2015.07.017.

Sides I. R., Edmonds M., Maclennan J., Houghton B. F., Swanson D. A. and Steele-MacInnis M. J. (2014) Magma mixing and high fountaining during the 1959 Kīlauea Iki eruption, Hawai'i. *Earth Planet. Sci. Lett.* **400**, 102–112. http://dx.doi.org/10.1016/j.epsl.2014.05.024.

Sinton C. W., Christie D. M., Coombs V. L., Nielsen R. L. and Fisk M. R. (1993) Near-primary melt inclusions in anorthite phenocrysts from the Galapagos Platform. *Earth Planet. Sci. Lett.* **119**, 527–537. http://dx.doi.org/10.1016/0012-821X(93)90060-M.

Sisson T. W. and Grove T. L. (1993) Experimental investigations of the role of H_2O in calc-alkaline differentiation and subduction zone magmatism. *Contrib. Miner. Petrol.* **113**, 143–166. http://dx.doi.org/10.1007/BF00283225.

Sobolev A. V. and Chaussidon M. (1996) H_2O concentrations in primary melts from supra-subduction zones and mid-ocean ridges: implications for H_2O storage and recycling in the mantle. *Earth Planet. Sci. Lett.* **137**, 45–55. http://dx.doi.org/10.1016/0012-821X(95)00203-O.

Sours-Page R. E., Nielsen R. L. and Batiza R. (2002) Melt inclusions as indicators of parental magma diversity on the Northern East Pacific Rise. *Chem. Geol.* **183**, 237–261. http://dx.doi.org/10.1016/S0009-2541(01)00384-9.

Steele-Macinnis M. J., Esposito R. and Bodnar R. J. (2011) Thermodynamic model for the effect of post-entrapment crystallization on the H_2O-CO_2 systematics of vapor-saturated, silicate melt inclusions. *J. Petrol.* **52**, 2461–2482. http://dx.doi.org/10.1093/petrology/egr052.

Stolper E. and Holloway J. R. (1988) Experimental determination of the solubility of carbon dioxide in molten basalt at low pressure. *Earth Planet. Sci. Lett.* **87**, 397–408. http://dx.doi.org/10.1016/0012-821X(88)90004-0.

Tait S. (1992) Selective preservation of melt inclusions in igneous phenocrysts. *Am. Mineral.* **77**, 146–155.

Thordarson T. (2014). The widespread ∼10 ka Saksunarvatn tephra is not the product of a single eruption. In American Geophysical Union, Fall Meeting. pp. V24B-04.

Thordarson T., Self S., Óskarsson N. and Hulsebosch T. (1996) Sulfur, chlorine, and fluorine degassing and atmospheric loading by the 1783–1784 AD Laki (Skaftár Fires) eruption in Iceland. *Bull. Volcanol.* **58**, 205–225. http://dx.doi.org/10.1007/s004450050136.

Thornalley D. J. R., McCave I. N. and Elderfield H. (2011) Tephra in deglacial ocean sediments south of Iceland: stratigraphy, geochemistry and oceanic reservoir ages. *J. Quat. Sci.* **26**, 190–198. http://dx.doi.org/10.1002/jqs.1442.

Toplis M. J. (2005) The thermodynamics of iron and magnesium partitioning between olivine and liquid: criteria for assessing and predicting equilibrium in natural and experimental systems. *Contrib. Miner. Petrol.* **149**, 22–39. http://dx.doi.org/10.1007/s00410-004-0629-4.

Tuffen H., Owen J. and Denton J. (2010) Magma degassing during subglacial eruptions and its use to reconstruct palaeo-ice thicknesses. *Earth Sci. Rev.* **99**, 1–18. http://dx.doi.org/10.1016/j.earscirev.2010.01.001.

Tugarinov A. I. and Naumov V. B. (1970) Dependence of the decrepitation temperature of minerals on the composition of their gas-liquid inclusions and hardness. *Academia Nauk SSSR Doklady* **195**, 112–114.

Waagstein R. (1968) Tre vulkanske askelage fra Fr. *Meddelelser fra Dansk Geol Foren* **18**, 257–264.

Wallace P. J., Kamenetsky V. S. and Cervantes P. (2015) Melt inclusion CO_2 contents, pressures of olivine crystallization, and the problem of shrinkage bubbles. *Am. Mineral.* **100**, 787–794.

Workman R. K., Hauri E. H., Hart S. R., Wang J. and Blusztajn J. (2006) Volatile and trace elements in basaltic glasses from Samoa: Implications for water distribution in the mantle. *Earth Planet. Sci. Lett.* **241**, 932–951. http://dx.doi.org/10.1016/j.epsl.2005.10.028.

Yu Y., Zhang Y., Chen Y. and Xu Z. (2016) Kinetics of anorthite dissolution in basaltic melt. *Geochim. Cosmochim. Acta* **179**, 257–274. http://dx.doi.org/10.1016/j.gca.2016.02.002.

Zhang Y., Ni H. and Chen Y. (2010) Diffusion data in silicate melts. *Rev. Mineral. Geochem.* **72**, 311–408. http://dx.doi.org/10.2138/rmg.2010.72.8.

Associate editor: Anders Meibom